The Astrophysical Journal, 952:44 (15pp), 2023 July 20 https://doi.org/10.3847/1538-4357/accea4

The Fraction and Kinematics of Broad Absorption Line Quasars across Cosmic Time

Manuela Bischetti[1,2], Fabrizio Fiore[2,3], Chiara Feruglio[2,3], Valentina D'Odorico[2,3,4], Nahum Arav[5], Tiago Costa[6], Kastytis Zubovas[7,8], George Becker[9], Sarah E. I. Bosman[10], Guido Cupani[2], Rebecca Davies[11,12], Anna-Christina Eilers[13], Emanuele Paolo Farina[14], Andrea Ferrara[4], Massimo Gaspari[15], Chiara Mazzucchelli[16], Masafusa Onoue[17,18], Enrico Piconcelli[19], Maria Vittoria Zanchettin[1,2,20], and Yongda Zhu[9]
[1] Dipartimento di Fisica, Universitá di Trieste, Sezione di Astronomia, Via G.B. Tiepolo 11, I-34131 Trieste, Italy; manuela.bischetti@units.it
[2] INAF—Osservatorio Astronomico di Trieste, Via G.B. Tiepolo 11, I–34143 Trieste, Italy
[3] IFPU—Institut for fundamental physics of the Universe, Via Beirut 2, I-34014 Trieste, Italy
[4] Scuola Normale Superiore, Piazza dei Cavalieri 7, I-56126 Pisa, Italy
[5] Department of Physics, Virginia Tech, Blacksburg, VA 24061, USA
[6] Max-Planck-Institut für Astrophysik, Karl-Schwarzschild-Straße 1, D-85748 Garching b. München, Germany
[7] Center for Physical Sciences and Technology, Saulétekio al. 3, Vilnius LT-10257, Lithuania
[8] Astronomical Observatory, Vilnius University, Saulétekio al. 3, Vilnius LT-10257, Lithuania
[9] Department of Physics & Astronomy, University of California, Riverside, CA 92521, USA
[10] Max-Planck-Institut für Astronomie, Königstuhl 17, D-69117 Heidelberg, Germany
[11] Centre for Astrophysics and Supercomputing, Swinburne University of Technology, Hawthorn, VIC 3122, Australia
[12] ARC Centre of Excellence for All Sky Astrophysics in 3 Dimensions (ASTRO 3D), Australia
[13] MIT Kavli Institute for Astrophysics and Space Research, 77 Massachusetts Avenue, Cambridge, MA 02139, USA
[14] Gemini Observatory, NSF's NOIRLab, 670 N A'ohoku Place, Hilo, HI 96720, USA
[15] Department of Astrophysical Sciences, Princeton University, Princeton, NJ 08544, USA
[16] Núcleo de Astronomía de la Facultad de Ingeniería, Universidad Diego Portales, Av. Ejército Libertador 441, Santiago, Chile
[17] Kavli Institute for Astronomy and Astrophysics, Peking University, Beijing 100871, People's Republic of China
[18] Kavli Institute for the Physics and Mathematics of the Universe (Kavli IPMU, WPI), The University of Tokyo, Chiba 277-8583, Japan
[19] INAF—Osservatorio Astronomico di Roma, via Frascati 33, 00040, Monte Porzio Catone, Italy
[20] SISSA, Via Bonomea 265, I-34136, Trieste, Italy
Received 2022 October 5; revised 2023 April 7; accepted 2023 April 18; published 2023 July 17

Abstract

Luminous quasars are powerful targets to investigate the role of feedback from supermassive black holes (BHs) in regulating the growth phases of BHs themselves and of their host galaxies, up to the highest redshifts. Here we investigate the cosmic evolution of the occurrence and kinematics of BH-driven outflows, as traced by broad absorption line (BAL) features, due to the C IV ionic transition. We exploit a sample of 1935 quasars at $z = 2.1$–6.6 with bolometric luminosity $\log(L_{\rm bol}/{\rm erg\ s^{-1}}) \gtrsim 46.5$, drawn from the Sloan Digital Sky Survey and from the X-Shooter legacy survey of Quasars at the Reionization Epoch (XQR-30). We consider rest-frame optical bright quasars to minimize observational biases due to quasar selection criteria. We apply a homogeneous BAL-identification analysis, based on employing composite template spectra to estimate the quasar intrinsic emission. We find a BAL quasar fraction close to 20% at $z \sim 2$–4, while it increases to almost 50% at $z \sim 6$. The velocity and width of the BAL features also increase at $z \gtrsim 4.5$. We exclude the possibility that the redshift evolution of the BAL properties is due to differences in terms of quasar luminosity and accretion rate. These results suggest significant BH feedback occurring in the 1 Gyr old universe, likely affecting the growth of BHs and, possibly, of their host galaxies, as supported by models of early BH and galaxy evolution.

Unified Astronomy Thesaurus concepts: Galaxy evolution (594); Spectroscopy (1558); Quasars (1319); Broad-absorption line quasar (183); Supermassive black holes (1663); High-redshift galaxies (734)

1. Introduction

Quasars are the brightest nontransient sources in the universe. They are powered by accretion onto supermassive black holes (BHs), whose emission typically dominates over the host-galaxy emission in the rest-frame UV and optical bands. High-redshift quasars at $z \simeq 2$–6.5 provide a unique window on the growth phases during which the most massive BHs and their host galaxies assembled the bulk of their mass (Marconi et al. 2004; Volonteri & Rees 2006). Luminous quasars at $z \gtrsim 2$, with bolometric luminosity $L_{\rm Bol} \sim 10^{47}$ erg s^{-1}, are typically powered by BHs with masses 10^8–10^{10} $M_\odot$ and high accretion rates $\lambda_{\rm Edd} = L_{\rm Bol}/L_{\rm Edd} \sim 0.01$–$1$ (e.g., Kurk et al. 2007; Shen et al. 2011; Mazzucchelli et al. 2017), where $L_{\rm Edd}$ is the Eddington luminosity. The large radiative output of these BHs is expected to drive powerful outflows, able to regulate the BH and host-galaxy growth, by injecting large amounts of energy and momentum in the galaxy interstellar medium (ISM; Zubovas & King 2012; Gaspari & Sadowski 2017; Menci et al. 2019).

BH-driven outflows in high-redshift quasars are often revealed by blueshifts of high-ionization emission lines with respect to the quasar systemic redshift (Meyer et al. 2019; Shen et al. 2019; Schindler et al. 2020) and from broad/asymmetric wings in the emission-line profiles (e.g., Zakamska et al. 2016; Kakkad et al. 2020). Another powerful tracer of BH-driven outflows are broad (>2000 km s^{-1}) absorption line (BAL) systems occurring in the rest-frame UV spectrum (Weymann et al. 1991), blueward of high-ionization emission lines such as C IV λ1549Å, Si IV λ1397Å, and N V λ1240Å (HiBAL), and of low-ionization emission lines such as Mg II λ2800Å

(LoBAL). BAL features have indeed been identified in quasars at all redshifts up to $z > 7$ (Wang et al. 2018, 2021b). Observational studies, mostly based on spectra from the Sloan Digital Sky Survey (SDSS), found that BAL outflows are observed in 10%–17% of $z \simeq 2$–4 quasars, and have typical velocities of 5000–10,000 km s^{-1} (Gibson et al. 2009; Pâris et al. 2018), although a few percent of them can reach 10%–15% of light speed (Hamann et al. 2018; Bruni et al. 2019; Rodríguez Hidalgo et al. 2020). LoBAL outflows are typically observed in a small fraction (10%–15%) of BAL quasars.

In luminous quasars at $z \simeq 2$–3, BAL outflows have been found to carry kinetic power values in the range 0.1%–10% of $L_{\rm Bol}$ (Dunn et al. 2010; Borguet et al. 2013; Byun et al. 2022), consistent with expectations for an efficient BH-feedback mechanism (Fiore et al. 2017). Similarly, galaxy evolution models identify BAL outflows as an important source of feedback (e.g., Costa et al. 2014; Torrey et al. 2020). Different scenarios for the launching and geometry of BAL outflows have been proposed (Elvis 2000; Proga et al. 2000; Proga & Kallman 2004; Xu et al. 2020; Zeilig-Hess et al. 2020). Although these winds are expected to originate within a parsec from the BH (Sadowski & Gaspari 2017), close to the accretion disk, observations indicate that BAL absorption in luminous quasars often occurs at much larger distances from the BH, that is, 100–1000 pc (Arav et al. 2018; Hemler et al. 2019). This suggests that these ionized outflows represent an important source of BH feedback on the growth of the BH itself and of the host galaxy.

At very high redshift ($z \gtrsim 6$), the occurrence and properties of BAL quasar outflows have been much less explored. The number of discovered BAL quasars has kept increasing with the growing number of quasars with spectroscopic observations of sufficient quality to probe at least the most prominent BAL features. A first guess for a BAL quasar fraction as high as 50% at $z \sim 6$ has been previously suggested by Maiolino et al. (2004), based on a very small sample of eight quasars. A BAL fraction of 16%–24% was later reported by Shen et al. (2019), Schindler et al. (2020), and Yang et al. (2021), although the BAL identification was mostly based on visual inspection and/or limited spectral range and signal-to-noise ratio (S/N) of the quasar spectra. In Bischetti et al. (2022), we performed the first systematic investigation of BAL outflows in 30 quasars at $5.8 \leqslant z \leqslant 6.6$ from the X-Shooter legacy survey of Quasars at the Reionization Epoch (XQR-30; Bosman et al. 2022; Zhu et al. 2021; Chen et al. 2022; Lai et al. 2022; Zhu et al. 2022), finding that about 47% of XQR-30 quasars show BAL features associated with C IV, a fraction that is ∼2.4 times higher than what is observed in $z \sim 2$–4 quasars. The majority of BAL outflows at $z \sim 6$ also show extreme velocities of 20,000–50,000 km s^{-1}, rarely observed at lower redshift. These findings are indication of an evolution in BAL properties between $z \simeq 2$ and $z \simeq 6$ quasars.

However, different factors such as $L_{\rm Bol}$ or $\lambda_{\rm Edd}$ are believed to affect the fraction of BAL quasars and their kinematics (e.g., Dai et al. 2008; Allen et al. 2011; Bruni et al. 2019). In this paper, we investigate the BAL fraction and the BAL kinematics' dependence on redshift and on quasar nuclear properties ($L_{\rm Bol}$, $\lambda_{\rm Edd}$), with the goal of identifying the main driver of the varying BAL properties. To this purpose, we measure the occurrence and kinematic properties of BAL outflows associated with the C IV ionic species in a sample of luminous quasars in the redshift range $z = 2.1$–6.6, with matched selection criteria, and by adopting a homogeneous BAL-identification analysis.

The paper is structured as follows. In Section 2, we describe the quasar sample, including the quasar selection criteria (Section 2.1). Section 3 details the BAL-identification analysis and compares it with previous approaches. The main results on the BAL fraction and on the BAL kinematics are presented in Sections 4 and 5, respectively. We discuss the cosmic evolution of the BAL properties and its implications for BH and galaxy evolution in Section 6. A summary and the main conclusions are given in Section 7. Throughout this paper, we adopt a Lambda cold dark matter cosmology with $H_0 = 67.3$ km s^{-1}, $\Omega_\Lambda = 0.69$, and $\Omega_M = 0.31$ (Planck Collaboration et al. 2016).

2. Quasar Sample

2.1. Quasar Selection

The observed fraction of BAL quasars with respect to non-BAL quasars is the convolution of the intrinsic BAL quasar occurrence and a quasar selection function. Standard quasar selection algorithms in optical surveys rely on multicolor imaging data which probe the rest-frame UV quasar spectrum at $z > 2$ (e.g., Richards et al. 2002). These UV colors can be affected by BAL troughs associated with high-ionization species such as C IV. In addition, BAL quasars typically show redder UV continua than non-BAL quasars (e.g., Reichard et al. 2003; Gibson et al. 2009). Depending on redshift, BAL quasars may thus show UV colors resembling those of stars, and may be more easily missed by spectroscopic samples than non-BAL quasars.

Aiming to measure the intrinsic fraction of BAL quasars across cosmic time, two main approaches can be followed. One possibility is to translate the observed BAL fraction ($f_{\rm obs}$) into an intrinsic fraction ($f_{\rm int}$) by correcting for selection effects. Previous attempts to correct for these effects, however, resulted in very different $f_{\rm int}$ (by a factor of 3), and different $f_{\rm obs}$ to $f_{\rm int}$ corrections (by a factor of 5), even considering the same set of selection effects and similar redshift intervals. When considering quasars from SDSS and from the Large Bright Quasar Survey, $f_{\rm int}$ ($f_{\rm obs}$) values in the range 13.4 (8.0)% to 40.7 (23%) have been reported, as summarized in Table 1. In all these cases, the derived $f_{\rm int}$ mostly depends on the adopted assumptions with regard to the input BAL properties, such as the distributions of the velocity, width, and depth of the absorption, and on the relation between the above quantities and reddening. The spread of plausible assumptions naturally leads to large uncertainties. The true $f_{\rm int}$ could in principle be derived by quantifying the selection effects on a set of synthetic spectra based on a physical model of BAL quasar outflows. Such an approach would nonetheless suffer from large uncertainties, due to the lack of a self-consistent physical model able to widely reproduce the properties of the BAL quasar population (e.g., Elvis 2000; Xu et al. 2020).

In this work, we follow a different approach that allows us to bypass the above issues. As we are mainly interested in the redshift evolution of the BAL fraction and kinematic properties, we apply a similar selection function at all redshifts. In particular, we consider rest-frame optically bright quasars to measure the BAL fraction in the redshift interval $z \simeq 2$–6.5. At $z \simeq 2$–4, the rest-frame optical band is probed by near-IR surveys such as the Two Micron All Sky Survey (2MASS; Skrutskie et al. 2006) and the UKIRT Infrared Deep Sky Survey (UKIDSS; Warren et al. 2007) in the H and K bands. For higher-redshift quasars ($z \sim 6$), a similar spectral coverage is provided by the Wide-field Infrared Survey Explorer (WISE;

Table 1
BAL Fraction Estimates at $2 < z < 4$

Reference (1)	$f_{\rm obs}$ (2)	$f_{\rm int}$ (3)
UV-selected quasars		
Reichard et al. (2003)	$14.0\% \pm 1.0\%$	$13.4\% \pm 1.2\%$
Knigge et al. (2008)	$13.7\% \pm 0.3\%$	$\leqslant 23\%$
Gibson et al. (2009)	$15.1\% \pm 0.6\%$	$18.5\% \pm 0.7\%$
Allen et al. (2011)	$8.0\% \pm 0.1\%$	$40.7\% \pm 5.4\%$
Hewett & Foltz (2003)	$15\% \pm 3\%$	$22\% \pm 4\%$
Optically selected quasars		
Dai et al. (2008)	$\sim 20\%$	$23\% \pm 3\%$
Ganguly & Brotherton (2008)	23%	...
Maddox et al. (2008)	17.5%	18.5%

Notes. (1) Reference, (2) observed BAL fraction, (3) intrinsic BAL fraction (see Section 2.1).

Wright et al. 2010) in the W1 and W2 bands (see Bischetti et al. 2022 for details). The rest-frame optical selection allows us to minimize selection effects by avoiding those biases generated by UV absorption troughs in the color selection. The $f_{\rm obs}$-to-$f_{\rm int}$ correction in rest-frame optical-selected quasars is indeed expected to be modest (10%–20%): Dai et al. (2008) found a $f_{\rm int} = 23\% \pm 3\%$ in the SDSS and 2MASS K-band bright quasars at $z \simeq 2$–4 ($f_{\rm obs} \sim 20\%$). This fraction is similar to that found by Ganguly et al. (2007) and Ganguly & Brotherton (2008) when combining SDSS and 2MASS catalogs (23%). Again, Maddox et al. (2008) reported a $f_{\rm int} = 18.5\%$ in SDSS and UKIDSS bright quasars, considering the fraction of quasars missed by the UKIDSS survey ($f_{\rm obs} = 17.5\%$). As a general trend, the observed BAL fraction calculated in rest-frame optical-selected quasars is roughly 50% higher than the BAL fraction observed in quasars selected only in the rest-frame UV: $f_{\rm obs}^{\rm optical} \simeq 1.5 \times f_{\rm obs}^{\rm UV}$. In addition, the observed and intrinsic BAL fractions calculated in rest-frame optical-selected quasars are similar. They are also similar to the intrinsic BAL fraction calculated in quasars selected only in the rest-frame UV: $f_{\rm obs}^{\rm optical} \simeq f_{\rm int}^{\rm optical} \sim f_{\rm int}^{\rm UV}$.

The $f_{\rm obs}$ of quasar samples selected from X-ray to radio surveys, affected by a variety of different selection effects, is typically lower or similar to 20% (e.g., Becker et al. 2000; Giustini et al. 2008), supporting the fact that an optical rest-frame selection limits selection biases against BAL quasars. In general, BAL fractions higher than 20% have been reported only (i) when considering the absorption index (AI; Hall et al. 2002) criterion to identify BAL quasars, instead of the so-called "balnicity index" criterion considered in this work (Weymann et al. 1991; see Section 3.2). The AI criterion identifies as BAL troughs the absorption features that are wider than 1000 km s^{-1}, and typically results in a 2 times higher BAL fraction than when using BI > 0 (Dai et al. 2008). Although the AI criterion can be used to identify the shallowest absorption features, it results in a large fraction of false BAL identifications when applied to spectroscopic data with modest spectral resolution (Knigge et al. 2008). In addition, (ii) BAL fractions higher than 20% have been reported in the reddest quasars (Urrutia et al. 2008; Glikman et al. 2012), which however constitute a minority ($\sim$10%) of the rest-frame optical-selected quasars.

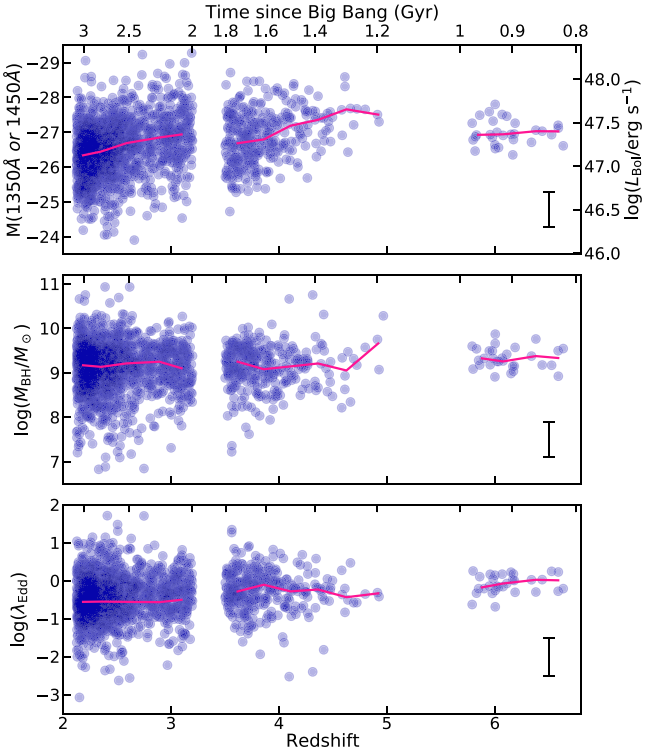

Figure 1. Absolute magnitude (top), BH mass (middle), and Eddington accretion rate (bottom) as a function of redshift for the quasar sample considered in this work. Top axis indicates time since the Big Bang. The magenta line represents the median magnitude in redshift bins $\Delta z = 0.25$. Error bars represent the typical uncertainties (see Sections 2.2 and 2.3).

Given the above evidence, the BAL fractions presented in this work and their redshift evolution are robust against selection effects.

2.2. 2.1 < z < 5.0 Sample

The low-redshift sample consists of 1578 quasars at $2.13 < z < 3.20$ from the catalog of SDSS Data Release 7 (DR7) quasars by Shen et al. (2011), selected to be detected by 2MASS in the H (1.7 μm) and K (2.2 μm) bands, which cover rest-frame optical regions of the quasar spectrum, similar to those probed by W1 and W2 in the high-redshift sample. We also include 327 SDSS DR7 quasars at $3.6 < z < 5.0$ from the Shen et al. (2011) catalog, requiring them to be detected in the 2MASS K band (which correspond to W1 at $z \sim 6$). These quasars are about a factor of 10 more luminous than the average SDSS quasar at $z > 2.13$, with a median magnitude of $M_{1450\text{Å}} = -26.6$ (-26.5 at $z < 3.2$, -26.9 at $3.6 < z < 5$; see Figure 1). Their spectra have a typical S/N ~ 18 per 70 km s^{-1} pixel in the 1500–1600 Å range. We derive $L_{\rm Bol}$ by applying a bolometric correction to the monochromatic luminosity of the rest-frame UV continuum (see Figure 1, with a typical scatter of $\sim$0.2 dex; Richards et al. 2006; Runnoe et al. 2012). This sample benefits from measured BH masses (Shen et al. 2011), which are based on the Mg II line for $z \lesssim 2.3$ quasars (349 quasars) and on the C IV emission line (1160 quasars) at $z > 2.3$, including the empirical correction for nonvirial motions by Coatman et al. (2017). We verified that the Mg II and C IV BH masses are consistent, for the 340 quasars in which both tracers are available, within the respective $\sim$0.3–0.5 dex uncertainties (e.g., Vestergaard & Osmer 2009), in agreement with the results of Shen et al. (2011). For the

subsample of quasars already discovered by SDSS Data Release 5 (DR5), the occurrence and properties of BAL outflows were investigated by Gibson et al. (2009), providing us with a reference analysis to test our BAL-identification method. For the remaining quasars, BAL identification in the catalog was based on visual inspection (Shen et al. 2011). In this work and in Bischetti et al. (2022), we have reanalyzed all SDSS quasars in the $2.1 < z < 5.0$ sample, following the approach described in Section 3.

2.3. $5.8 < z < 6.6$ Sample

The high-redshift sample used in this work consists of 30 luminous quasars (median AB magnitude $M_{1450\text{Å}} = -26.9$) at $5.8 \lesssim z \lesssim 6.6$ from the XQR-30 survey. Their magnitude and redshift distributions are shown in Figure 1 (Bañados et al. 2016; Mazzucchelli et al. 2017; Reed et al. 2017; Decarli et al. 2018; Wang et al. 2019; Eilers et al. 2020). These quasars are selected to be bright in both the rest-frame UV (AB magnitude $J \leqslant 19.8$ for $z < 6.0$ sources and $J \leqslant 20.0$ for quasars at $z \geqslant 6.0$) and in the rest-frame optical, being all detected by WISE in the W1 (3.4 μm) and W2 (4.6 μm) bands (Bañados et al. 2016; Ross & Cross 2020). Further details about the selection of XQR-30 quasars, data reduction of the X-Shooter spectra, and the target list are given in Bischetti et al. (2022). This sample benefits from deep X-Shooter observations (S/N $\gtrsim$ 25 per 50 km s^{-1} pixel in the rest-frame spectral range 1600–1700 Å), and robust, Mg II-based BH masses (Lai et al. 2022). As for the low-redshift sample, we verified the consistency between Mg II- and C IV-based BH masses. Bolometric luminosities are computed via rest-frame UV bolometric correction using the same method applied to the low-redshift sample (Runnoe et al. 2012).

A systematic search and characterization of C IV BAL outflows in XQR-30 was performed in Bischetti et al. (2022), based on the same approach used in this work (Section 3). Although X-Shooter spectra of similar quality (S/N $\gtrsim$ 10) exist to date for several luminous quasars at $5.0 < z < 5.4$, we do not consider them in this work as they have been mostly selected for studies of intervening absorbers and are therefore biased against the presence of BAL features (Becker et al. 2019).

3. Identification of Broad Absorption Line Quasars

3.1. Reconstruction of Quasar Continuum Emission

To search for BAL absorption troughs, the first step is to model the intrinsic continuum emission in the rest-frame UV. A possible approach is to fit the spectra with a quasar emission model accounting for continuum and line emission, and extrapolating this model to the spectral region affected by the BAL (Figure 2). Models typically include a power-law component to reproduce the quasar continuum emission, and Voigt or Gaussian profiles to account for emission lines (Gibson et al. 2009; Shen et al. 2011, 2019). Alternatively, more complex, nonphysically motivated functions such as splines are sometimes used, as they can be more flexible in reproducing a variety of quasar spectra (e.g., Bruni et al. 2019). Both approaches require that a sufficiently large portion of the quasar spectrum is free from both absorption and emission lines, allowing one to anchor the fit. However, this condition is often unsatisfied in the spectral region between Lyα and C IV, resulting in large uncertainties (Figure 2). In addition, both methods are largely dependent on the regions of the spectrum that are masked prior to fitting, especially in those cases where

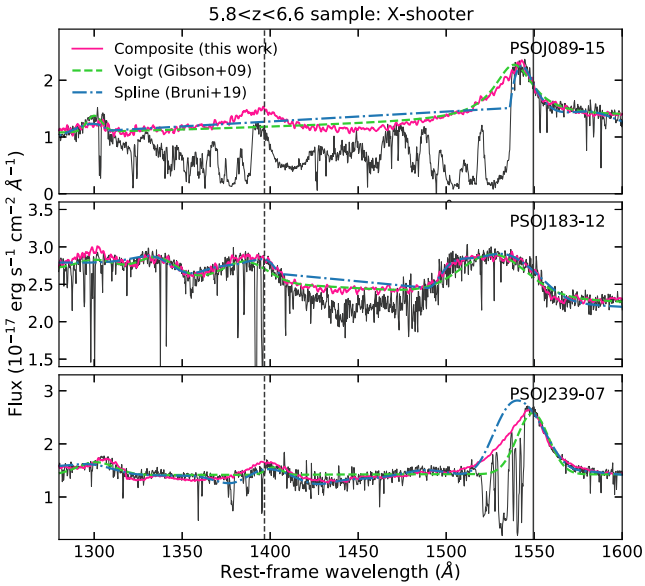

Figure 2. Example of three BAL quasars from the $5.8 < z < 6.6$ sample considered in this work. We show the comparison between our estimate of the intrinsic quasar emission, based on composite template spectra (Section 3.1), with the quasar emission model by Gibson et al. (2009) and the spline model by Bruni et al. (2019). Vertical solid and dashed lines refer to the rest-frame wavelength of C IV and Si IV, respectively.

BAL features cover a wide spectral range or affect emission-line profiles.

These uncertainties can be minimized using composite templates built from observed quasar spectra. Quasar spectra can be combined via different techniques such as principal component analysis (Trump et al. 2006; Pâris et al. 2018; Guo & Martini 2019) or nonnegative matrix factorization (Allen et al. 2011). Here we build, for each quasar of the sample, a composite template based on a large number of SDSS quasar spectra classified as non-BAL in Gibson et al. (2009), each matching within ±20% its color and the equivalent width (EW) of the C IV line (Shen et al. 2011). Given the anticorrelation between the EW of C IV and its blueshift with respect to the quasar redshift due to outflowing gas motions (Coatman et al. 2017; Vietri et al. 2018), the latter criterion allows us to reproduce all levels of asymmetry in the C IV line profile. A similar approach was recently adopted by Wang et al. (2018, 2021b), who created composite templates based on matching the C IV blueshift of two $z > 7$ BAL quasars. The C IV EW or the blueshift criteria should in principle produce similar composite templates. However, SDSS quasar redshifts rely on automatic fitting procedures based on a limited spectral coverage, and are therefore affected by uncertainties on the C IV blueshift that can reach thousands of kilometers per second, leading to an inaccurate selection of the quasar spectra contributing to the template. We find that a better spectrum–template agreement can be achieved by using the C IV EW during the selection of the quasar spectra.

Concerning the quasar colors, we consider the F (1700 Å)/F (2100 Å) flux ratio to reproduce the continuum slope redwards of C IV, and the F (1290 Å)/F (1700 Å) flux ratio to account for a change in the continuum slope as observed in red quasar spectra (e.g., Trump et al. 2006; Shen et al. 2019). We calculate F (1700 Å) and F (2100 Å) as median flux values over 100 Å and F (1290 Å) over 30 Å in the rest frame. The underlying assumption is that the observed and intrinsic continuum emission do not differ

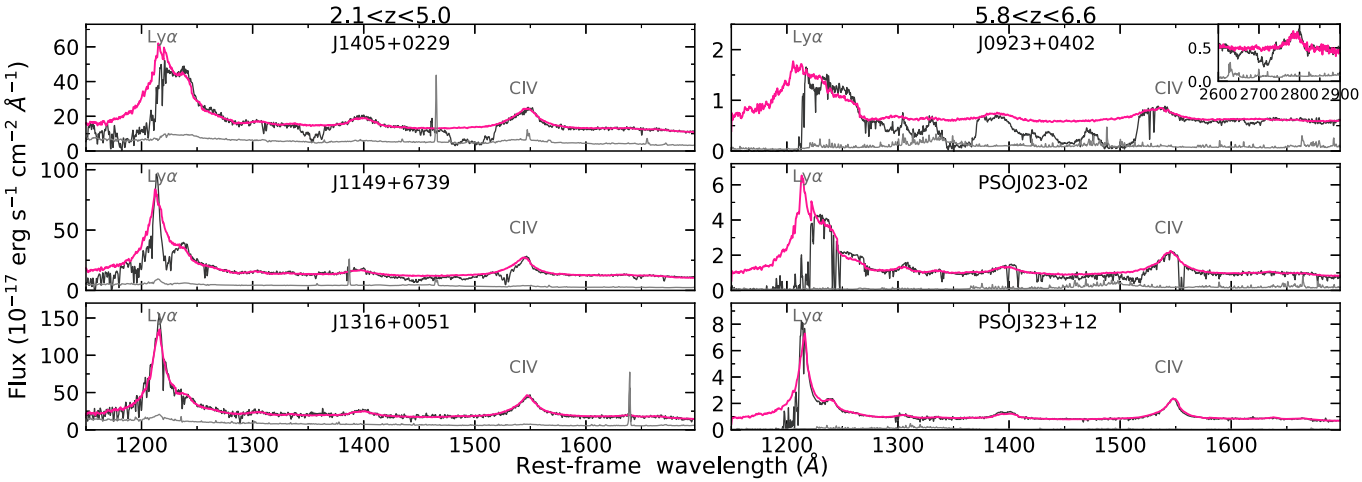

Figure 3. Examples of BAL (top and middle) and non-BAL (bottom) quasar spectra, randomly selected from our sample and binned to 50 km s^{-1} (black curves). Left (right) column shows SDSS (X-Shooter) spectra. In the case of J0923+0402 ($z = 6.626$), the inset displays the spectral region close to Mg II affected by BAL features. Composite templates, used to estimate the intrinsic quasar emission, are shown by the magenta curve (Section 3.1). We also show in gray the flux uncertainty multiplied by a factor of 5. Labels indicate the Lyα and C IV emission lines.

around 1290 Å, that is, the bluest spectral region, redward of Lyα, free from strong emission lines. In fact, Lyα forest absorption complicates our measure of the $\lambda < 1216$ Å quasar continuum, owing to the absorption becoming stronger with increasing redshift. In the case that BAL absorption troughs affect the spectral region close to 1290 Å, our approach would provide a lower limit on the intrinsic quasar continuum emission and on the absorption BI (Section 2).

Starting from the total Shen et al. (2011) catalog of 11,800 SDSS quasars in the redshift range $2.13 < z < 3.20$, for which SDSS spectroscopy probes the 1216–2100 Å wavelength range, the composite template spectrum is built as the median of a hundred randomly selected, non-BAL (Gibson et al. 2009; Shen et al. 2011) quasar spectra. The above number is a trade-off between using stringent selection criteria and ensuring that the composite template is not affected by individual quasar spectra. The composite template is normalized to the median flux value of the quasar spectrum in the rest-frame 1650–1750 Å spectral interval, avoiding prominent emission lines and strong telluric absorption for the redshift interval covered by our sample (Smette et al. 2015). Figure 2 shows that the above approach provides us with (i) a solid reconstruction of the C IV profile even when affected by strong absorption features, (ii) a reasonable estimate of the quasar emission blueward of C IV also in the most absorbed spectra, and (iii) a conservative estimate of the continuum emission, typically lower or similar to the continuum reproduced by the Gibson et al. (2009) and Bruni et al. (2019) models. Figure 3 shows examples of the SDSS and X-Shooter spectra for the quasars belonging to the $2.1 < z < 5.0$ and $5.8 < z < 6.6$ samples, respectively. The X-Shooter spectra and composite templates for the remaining $5.8 < z < 6.6$ quasars are shown in the Appendix in Figure 11. Normalized spectra are obtained by dividing each spectrum by its matched composite template (Figure 4).

3.2. Characterization of Broad Absorption Line Troughs

The standard indicator used to identify absorption features in quasar spectra due to BAL outflows is the balnicity index (BI), first introduced by Weymann et al. (1991), which is a modified EW of the BAL absorption and is less affected by false BAL identification than the AI criterion (Knigge et al. 2008). Here we adopt the BI definition by Gibson et al. (2009):

$$\mathrm{BI} = \int_0^{v_{\rm lim}} \left(1 - \frac{f(v)}{0.9}\right) C dv, \quad (1)$$

where $f(v)$ is the normalized spectrum, $C = 1$ if $f(v) < 0.9$ for contiguous troughs of >2000 km s^{-1}, and $C = 0$ otherwise. The $f(v) < 0.9$ threshold identifies as BAL features only the spectral regions dipping by 10% or more below the quasar continuum level, and represents a trade-off between taking into account typical uncertainties on the level of the modeled quasar continuum and including shallow absorption features (Weymann et al. 1991).

We search the normalized spectra for BAL features in the region between Lyα and C IV, that is, corresponding to $v_{\rm lim} \sim$ 64,000 km s^{-1} for C IV BAL outflows, ~35,000 km s^{-1} for Si IV, and ~6000 km s^{-1} for N V, respectively. We do not extend the search to smaller wavelengths due to the stronger intergalactic medium absorption blueward of Lyα with increasing redshift, preventing us from a homogeneous BAL identification at different epochs. We identify the minimum ($v_{\rm min}$) and maximum ($v_{\rm max}$) BAL velocity for a given transition, as the lowest and highest velocity for which $C = 1$ in Equation (1), respectively. Previous studies have been typically limited to $v_{\rm lim} = 25{,}000$ km s^{-1} (Trump et al. 2006; Gibson et al. 2009; Guo & Martini 2019), to avoid discriminating between BAL outflows associated with C IV and Si IV ions. Here we exploit the fact that the C IV optical depth is usually similar to or larger than the Si IV depth in BAL quasars (Dunn et al. 2012). This allows us to use the velocity range of the C IV BAL troughs to identify absorption associated with Si IV (Figure 4; see also Wang et al. 2018; Bruni et al. 2019). This implies that absorption features blueward of Si IV are due to a low-velocity Si IV BAL if a C IV BAL with similar velocity is observed. Otherwise, these features are considered to be produced by a high-velocity ($v_{\rm max} \gtrsim$ 30,000 km s^{-1}) C IV BAL (see also Rodríguez Hidalgo et al. 2020). We similarly assume that the C IV optical depth is larger than those of Mg II and N V and apply the methodology above to identify Mg II and BAL features. We measure the BAL width, defined as $w_{\rm max} = v_{\rm max} - v_{\rm min}$. The distributions of BI, $v_{\rm min}$, and $v_{\rm max}$ for the C IV BAL quasars identified in our sample are shown in Figure 2 of Bischetti et al. (2022), and values for

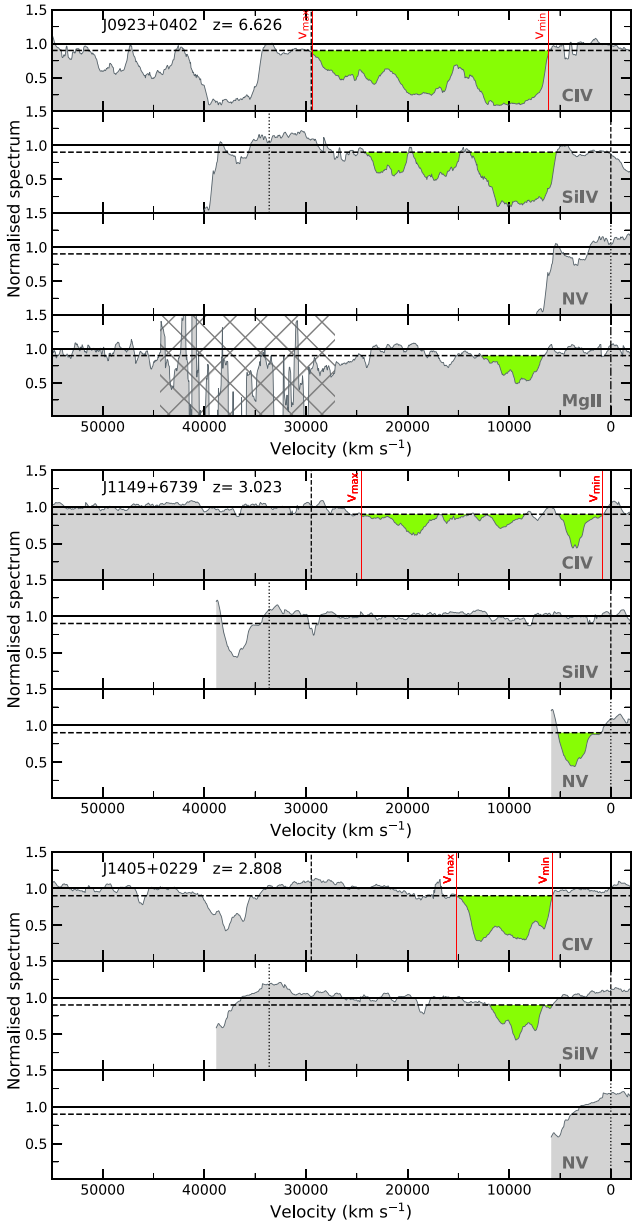

Figure 4. Examples of normalized spectra for three BAL quasars in our sample, smoothed to 500 km s^{-1}. The velocity axis in each panel is relative to the rest-frame wavelength of the ionic species indicated by the label. Vertical solid, dashed, dotted, and dashed–dotted lines indicate the velocity associated with the C IV, Si IV, N V, and Mg II emission lines, respectively. The solid (dashed) horizontal line represents a flux level of 1.0 (0.9). BAL troughs, corresponding to a flux level <0.9 (Equation (1)), are highlighted as green shaded areas. Vertical red lines indicate v_{max} and v_{min} for the C IV BAL. The hatched area indicates the spectral region affected by strong telluric features.

individual quasars at $5.8 < z < 6.6$ are listed in their Table E1. Uncertainties on the BAL parameters have been computed taking into account the uncertainty on both slope and normalization of the best-fit composite template, following the method in Bischetti et al. (2022). Briefly, we created for each quasar a bluer and a redder template as the median of the 33% bluest and the 33% reddest spectra contributing to the best-fit template, and we used them to create new normalized spectra, from which the range of variation of the BAL parameters is calculated. The median uncertainties (68% confidence level) on BI, v_{min}, v_{max}, and w_{max} are 310, 200, 380, and 340 km s^{-1}, respectively, while uncertainties for individual quasars in the $5.8 < z < 6.6$ sample are given in Table 2. We note that adopting a lower threshold of ∼0.8 in Equation (1) would identify as a BAL only the deepest absorption features (corresponding to a BI $\gtrsim$ 1000 km s^{-1}), and would typically imply lower v_{max}(higher v_{min}) by ∼1000–2000 km s^{-1}.

Table 2
Si IV and N V BAL Parameters

Name (1)	Species (2)	BI (3)	v_{min} (4)	v_{max} (5)
PSOJ009−10	Si IV	2880^{+750}_{-160}	$33{,}040^{+220(*)}_{-110}$	$38{,}360^{+150(*)}_{-1360}$
PSOJ065+01	Si IV	660^{+430}_{-150}	$17{,}240^{+130}_{-210}$	$27{,}190^{+1030}_{-510}$
PSOJ089−15	Si IV	8150^{+710}_{-620}	2280^{+150}_{-120}	$28{,}040^{+160}_{-220}$
	N V	2280^{+190}_{-280}	2270^{+150}_{-110}	$5{,}870^{(**)}_{-170}$
J0923+0402	Si IV	7970^{+230}_{-150}	6110^{+150}_{-150}	$24{,}330^{+350}_{-200}$
PSOJ217−07	Si IV	440^{+170}_{-150}	$30{,}460^{+270}_{-120}$	$35{,}000^{+430}_{-100}$
PSOJ231−20	N V	630^{+230}_{-190}	140^{+130}_{-210}	2350^{+160}_{-140}
PSOJ239−07	Si IV	230^{+310}_{-120}	830^{+160}_{-120}	3360^{+1010}_{-120}
	N V	$1{,}810^{+130}_{-100}$	820^{+100}_{-120}	5720^{+110}_{-100}
J2211−3206	Si IV	3420^{+130}_{-110}	9550^{+290}_{-470}	$19{,}120^{+350}_{-140}$
J2250−5015	Si IV	1320^{+170}_{-110}	$29{,}460^{+150}_{-810}$	$37{,}540^{+170}_{-130}$

Notes. (1) Quasar ID, (2) ionic species of the BAL, (3–5) balnicity index, minimum and maximum velocity of the Si IV BAL outflows, in units of kilometers per second. Positive v_{min} and v_{max} values indicate blueshifted absorption. (*) We assume the same range of v_{min} and v_{max} of the C IV BAL (Bischetti et al. 2022). (**) v_{max} corresponds to rest-frame 1216 Å, below which the spectrum is dominated by Lyα forest absorption (Section 3).

3.3. Non-C IV Broad Absorption Line Quasars in the XQR-30 Sample

Although the identification of BAL features in high-redshift quasars is mostly based on C IV, due to its high optical depth, the combined study of several other ionic species can be used to investigate the ionization level, kinematic structure, and column density of the outflow (e.g., Filiz et al. 2014; Baskin et al. 2015). However, only a few cases of non-C IV BAL outflows at $z \gtrsim 6$ have been reported so far (Wang et al. 2018, 2021b).

Here we find that, of the 14 C IV BAL quasars identified in Bischetti et al. (2022), eight also show a BAL system associated with the Si IV ion (namely, PSOJ009-10, PSOJ065+01, PSOJ089-15, J0923+0402, PSOJ217-07, PSOJ239-07, J2211-3206, and J2250-5015), three show a N V BAL (namely, PSOJ089-15, PSOJ231-20, and PSOJ239-07), and one (J0923+0402) shows a Mg II BAL. Figure 4 shows as an example the normalized spectrum of quasar J0923+0402 at $z \sim 6.6$, for which we identify strong BAL systems associated with C IV, Si IV, and Mg II ions. The C IV BAL is characterized by a BI (C IV) = 15,370 km s^{-1} and extends between v_{min}(C IV) = 6090 km s^{-1} and v_{max}(C IV) =29,500 km s^{-1} (Bischetti et al. 2022). We identify a Si IV BAL spanning a similar velocity range, with BI (Si IV) = 7390 km s^{-1}, and a less prominent Mg II BAL with BI (Mg II) = 2340 km s^{-1}. We cannot assess the presence of a N V BAL in this quasar, because of almost no transmitted flux blueward of Lyα.

We thus classify 12 quasars as HiBALs, and quasar J0923+0402 ($z \simeq 6.63$) as a LoBAL. In the case of PSOJ189-15 ($z \simeq 5.97$), strong telluric contamination affecting the spectral region blueward of Mg II does not allow us to validate/rule out the presence of a Mg II BAL. Our results increases by a factor of about 4 the number of Si IV BAL quasars identified at $z \gtrsim 6$

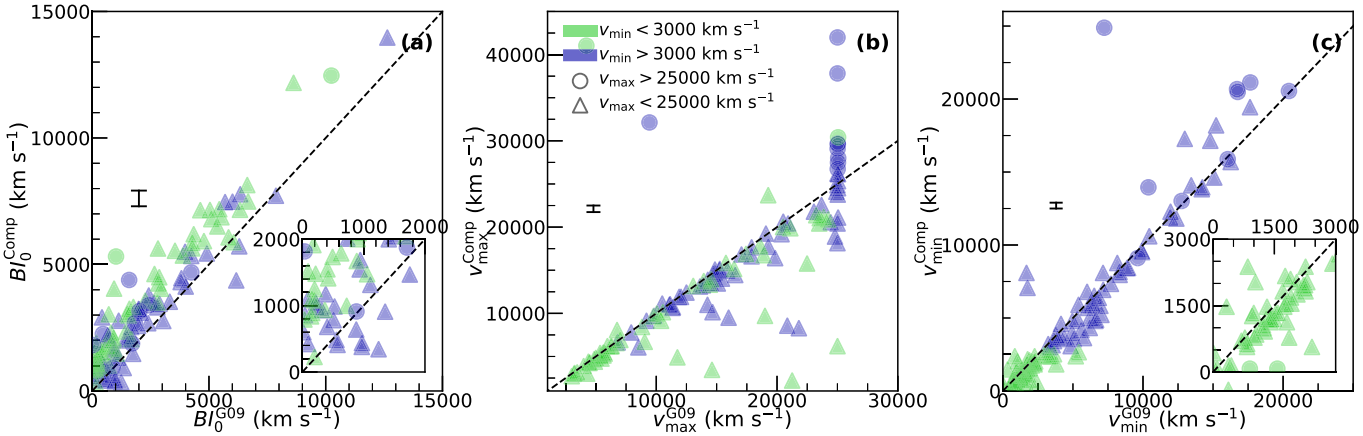

Figure 5. Comparison between the C IV BAL properties measured with our composite template method, labeled as "Comp" (Section 3.1), and in the analysis by Gibson et al. (2009) for the quasars in the $2.1 < z < 5.0$ sample, labeled as "G09." (a) Balnicity index BI, (b) maximum velocity v_{max}, and (c) minimum velocity v_{min} of the BAL outflows. In panels (a) and (c), the inset is a zoom in of the region with small BI and v_{min}, respectively. In all panels, the dashed line indicates a 1:1 relation and the error bar represents the typical uncertainty on the BAL parameters (Section 3.2).

(Wang et al. 2021b). The presence of a Si IV BAL in J2211-3206 ($z = 6.33$) was previously suggested by Chehade et al. (2018). A few hints of Mg II absorption in $z \gtrsim 6$ quasars have been reported so far (e.g., Maiolino et al. 2004; Wang et al. 2021b).

The BAL parameters measured for the Si IV and N V BAL outflows are listed in Table 2, and their residual spectra are shown in the Appendix in Figure 12. The Si IV BAL features are characterized by a BI $\sim$ 200–8100 km s^{-1}, which are typically smaller (10%–60%) than those measured in C IV, consistently with what has been found for SDSS quasars (Gibson et al. 2009). The only exception is PSOJ009-10, for which BI (C IV) = 1110 km s^{-1} (Bischetti et al. 2022) and BI (Si IV) = 2880 km s^{-1}. However, this quasar shows a very red spectrum with almost no Lyα and N V emission, overfitted by the composite template at $\lambda < 1270$ Å (Figure 11 in the Appendix). This suggests strong absorption, consistent with the presence of a Si IV BAL outflow, whose properties are nevertheless highly uncertain. For the N V BALs, we measure BI $\sim$600–2300 km s^{-1}.

3.4. Reanalysis of Sloan Digital Sky Survey Quasar Spectra

Given that the $2.1 < z < 5.0$ quasars in our sample did not benefit from a homogeneous identification and characterization of BAL outflows from the literature (Section 2.2), we have reanalyzed their spectra following the approach described in Section 3. In Figure 5, we compare our results with those by Gibson et al. (2009), who provided BI, v_{min}, and v_{max} for the 1317 SDSS DR5 quasars in our sample (Schneider et al. 2007). We identify as BALs 162 out of the 207 BAL quasars found by Gibson et al. (2009). The remaining quasars, classified as non-BAL quasars in our analysis, have only very weak BAL absorption in Gibson et al. (2009; all but five have BI < 500 km s^{-1}), likely owing to the flat continuum emission in the C IV–Si IV spectral region not being well reproduced by the reddened power-law continuum model used by Gibson et al. (2009), introducing a small systematic on the true continuum level. One example is shown in Figure 6 (top panel) for quasar SDSSJ1215+0906 ($z = 2.72$), previously classified as a BAL quasar with a BI $\simeq$ 120 km s^{-1} by Gibson et al. (2009), which we instead identify as a non-BAL. In addition, small differences between the DR5 and DR7 spectra can easily produce BI variations of a few hundred kilometers per second (e.g., Byun et al. 2022; Vietri et al. 2022). On the other hand, we identify 39 new BAL quasars that were classified as non-BALs by Gibson et al. (2009). One example is SDSS quasar J1432+1139 ($z = 2.99$; see Figure 6, middle panel), showing high-velocity C IV BAL features with $v_{min} \sim$ 29,000 km s^{-1}, that is, outside the spectral range investigated by Gibson et al. (2009). When comparing the properties of the BAL quasars identified in both our work and Gibson et al. (2009), we find on average no systematic difference in BI, with a significant scatter at BI $\lesssim$ 1000 km s^{-1} (Figure 5(a)). We measure higher BI for those quasars in which the BAL absorption reaches $v_{max} >$ 25,000 km s^{-1}, as Gibson et al. (2009) did not account for absorption troughs beyond this threshold. We typically measure larger BI in those cases in which the absorption has $v_{min} <$ 3000 km s^{-1} and thus affects the blue side of the C IV line, as it can be seen for SDSS J2238-0808 ($z = 3.17$) in Figure 6 (bottom panel). This is due to the fact that our composite templates better reproduce the asymmetric C IV profiles, typically showing a more prominent blue wing due to ionized outflows, than the Voigt profiles in Gibson et al. (2009).

The majority of the C IV BAL outflows show v_{max} and v_{min} velocities similar to those measured by Gibson et al. (2009). In a few cases, we measure lower v_{max} because of the different continuum treatments, and we identify a subsample of BAL quasars with extremely fast BAL outflows ($v_{max} \sim$ 25,000–40,000 km s^{-1}), missed by Gibson et al. (2009). These high-velocity BAL outflows are visible as a cutoff around $v_{max}^{G09} \sim$ 25,000 km s^{-1} in Figure 5(b). Our findings are consistent with the results of Bruni et al. (2019) and Rodríguez Hidalgo et al. (2020), who reported the presence of BAL outflows reaching velocities of 10%–15% of the light speed in a small fraction of SDSS quasars at $z \sim$ 2–4. In the case of absorption with $v_{min} <$ 3000 km s^{-1} (Figure 5(c)), we typically measure v_{min} lower by a factor of about 2 with respect to Gibson et al.'s (2009) estimates, likely because the Voigt profiles employed in their modeling underestimate the intrinsic emission of the C IV blue wing (Figure 6, bottom).

4. Broad Absorption Line Quasar Fraction

Figure 7 shows the evolution of the BAL quasar fraction across a cosmic time interval of about 2.3 Gyr, corresponding to the redshift range $2.1 < z < 6.6$ probed by our sample. We find the BAL fraction to be almost constant at $z \lesssim 4.5$, with

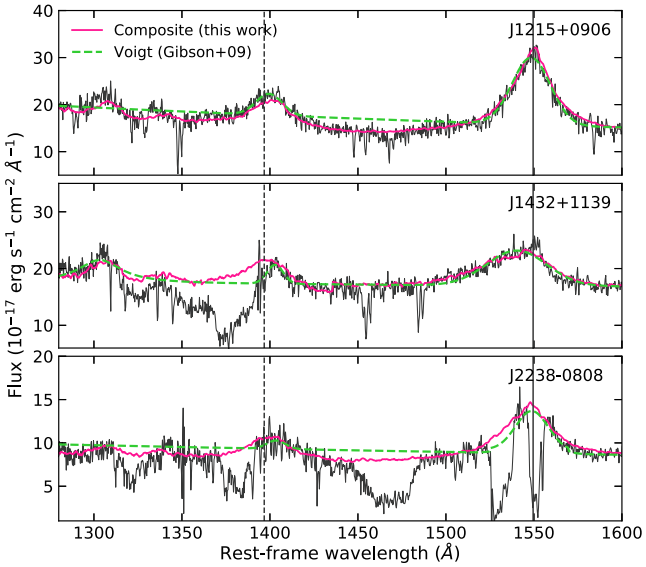

Figure 6. Example of SDSS spectra for three BAL quasars from the $2.1 < z < 5.0$ sample. We show a comparison between our reconstruction of the intrinsic quasar emission, based on composite template spectra (Section 3.1), and the prescription by Gibson et al. (2009). Different recipes can lead to a different BAL/no-BAL classifications (J1215+0906 and J1432 +1139), and to a different BI (J2238-0808); see Section 3.4 for details. Vertical solid and dashed lines refer to the rest-frame wavelength of C IV and Si IV, respectively.

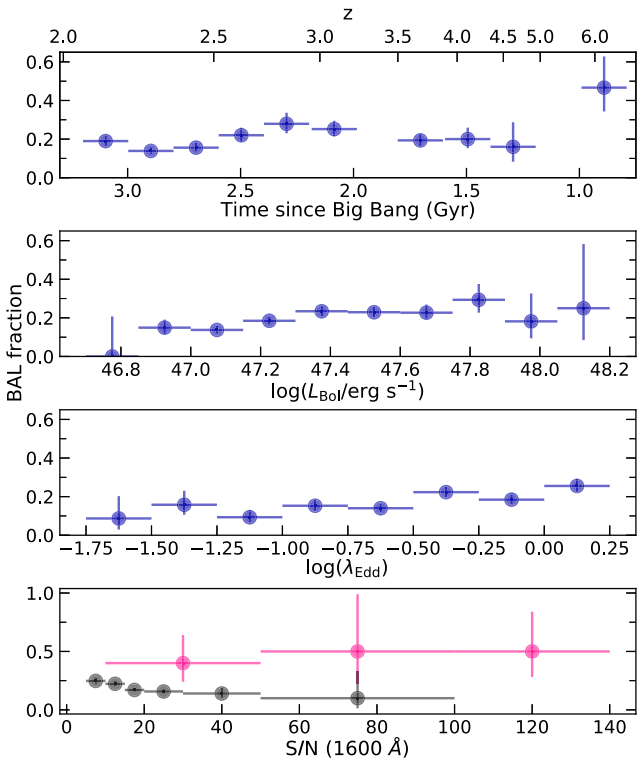

Figure 7. BAL fraction as a function of different physical quantities. Top: cosmic time, from 0.8 to 3.2 Gyr from the Big Bang, in bins of ∼200 Myr. The top axis indicates the corresponding redshift interval. Second from top: quasar bolometric luminosity, estimated from the rest-frame optical via bolometric correction. Second from bottom: accretion rate. Bottom: median S/N of the quasar continuum at rest-frame 1600 Å (Section 4). Black (magenta) dots refer to the $2.1 < z < 5.0$ ($5.8 < z < 6.6$) sample. In each panel, the horizontal bars indicate the bins in which BAL fractions have been calculated, while vertical bars show Poissonian uncertainties at a 90% confidence level for each bin (Gehrels 1986).

a median value of ∼20%. The oscillations around this value are likely due to the SDSS quasar selection systematics affecting differently BAL and non-BAL quasars as a function of redshift, which are minimized but not totally removed by our sample selection (Section 2.1). Indeed, BAL quasars are expected to be less efficiently selected than non-BALs at $z < 2.5$, more efficiently selected at $2.6 < z < 3.1$, while no significant difference in the selection efficiency is predicted for $3.1 < z < 3.5$ (Reichard et al. 2003). The BAL fraction is instead significantly higher at $z \gtrsim 6$, by a factor of about 2.5 (Bischetti et al. 2022). The lack of data at $z \sim 5$ does not allow us to assess whether the decrease in the BAL fraction at $z < 6$ is smooth, consistent with secular evolution of the BH accretion properties, or whether it rapidly drops after $z \sim 6$, due to efficient BH feedback at early epochs (see Section 6.1).

To investigate whether the BAL fraction depends on the nuclear properties of the quasar, Figure 7 also shows the BAL fraction as a function of L_{Bol} and λ_{Edd}. Bischetti et al. (2022) found no significant increase in the BAL fraction of $z \sim 2$–4 quasars in the luminosity range $\log(L_{Bol}/\mathrm{erg\ s^{-1}}) \simeq 46.5$–48, even after correcting the UV-continuum level for the BAL absorption. However, because BAL quasars typically show redder slopes of the UV continuum (Trump et al. 2006; Gibson et al. 2009; Allen et al. 2011) also in the high-luminosity regime spanned by our sample, using a common bolometric correction may result in an underestimate of L_{Bol} in BAL quasars. We do not correct the continuum luminosity for dust extinction because of the limited spectral range covered by the SDSS spectra, resulting in substantial degeneracy between the UV-continuum shape and the magnitude of intrinsic reddening (e.g., Gibson et al. 2009). Also, one would need to assume an extinction law and possibly also its evolution with redshift (e.g., Gallerani et al. 2010), increasing the uncertainties on L_{Bol}. Instead, because all quasars in our sample are detected in the rest-frame optical, we derive an independent estimate of L_{Bol} by applying the ∼5100 Å bolometric correction by Runnoe et al. (2012) to the 2MASS $H(K)$ fluxes for the $2.13 < z < 3.2$ ($3.6 < z < 5.8$) subgroups in our low-z sample, and to the WISE W1 fluxes for the high-z sample. The optical-based and UV-based bolometric luminosities are consistent for non-BAL quasars, while the optical-based L_{Bol} are typically higher by a factor of 2 for BAL quasars. Figure 7 shows the BAL fraction as a function of the optical-based L_{Bol}. We find a marginal correlation (p-value ∼0.05–0.09; Table 3) with a BAL fraction increase from ∼20% to 25%. A clearer trend (p-value ∼0.009–0.03) is observed between the BAL fraction and λ_{Edd}, with a factor of 2 increase in the BAL fraction for $\log\lambda_{Edd} \in [-1.7, 0.2]$ up to ∼25%, although we caution that most of the BH masses for our $2.1 < z < 5.0$ are based on the C IV line width, which can be significantly altered by the presence of BAL absorption with velocities of a few thousands of kilometers per second. This is consistent with the results from previous studies focusing on luminous quasars at $z \sim 2$–4 (Dai et al. 2008; Bruni et al. 2019). Nevertheless, neither the L_{Bol} nor the λ_{Edd} trends can account for the ∼47% BAL fraction measured for the $5.8 < z < 6.6$ sample (median $\log(L_{Bol}/\mathrm{erg\ s^{-1}}) = 47.3$, median $\lambda_{Edd} = -0.10$).

Finally, we investigate the dependence of the BAL fraction on the S/N of the quasar spectra. To this purpose, we homogeneously compute the S/N as the ratio between the median quasar continuum emission in the rest-frame interval 1650–1750 Å and the spectral noise, defined as the median rms in the same spectral region for a 70 km s^{-1} pixel (Section 3.1). Figure 7 (bottom)

Table 3
Results from χ^2 and Spearman's Rank Statistical Tests

Correlation	p-value$_{\chi^2}$ (1)	p-value$_S$ (2)
BAL fraction versus $L_{\rm Bol}$	0.05 [0.03–0.08]	0.09 [0.02–0.52]
BAL fraction versus $\lambda_{\rm Edd}$	0.009 [0.002–0.05]	0.03 [0.008–0.11]
$v_{\rm max}$ versus z	1.3×10^{-10}	2.0×10^{-4}
$v_{\rm min}$ versus z	0.025	0.016
$w_{\rm max}$ versus z	6.9×10^{-5}	9.5×10^{-4}
$v_{\rm max}$ versus $\lambda_{\rm Edd}$	0.16 [0.06–0.43]	0.045 [0.009–0.24]
$v_{\rm min}$ versus $\lambda_{\rm Edd}$	0.81 [0.61–1.0]	0.45 [0.28–0.71]
$w_{\rm max}$ versus $\lambda_{\rm Edd}$	0.03 [0.004–0.1]	0.01 [0.002–0.07]

Notes. (1) p-values associated with the χ^2 difference between a constant and a linear-relation fit. (2) p-values for a Spearman's rank correlation test. Square brackets correspond to the standard deviation on p, taking into account the 0.2 (0.5) dex uncertainty on $L_{\rm Bol}(\lambda_{\rm Edd})$.

shows no trend of the BAL with S/N for the $5.8 < z < 6.6$ sample, while it decreases with increasing S/N for the $2.1 < z < 5.0$ sample. This is likely due to the combination of (i) a similar rms sensitivity for the spectra, and (ii) bluer continuum slopes, translating into higher S/N for the non-BAL quasars in our sample. Previous studies of BAL quasars in SDSS reported no or little increasing trend (a few percent) of the BAL fraction with S/N, for a similar range of S/N = 10–50 (Gibson et al. 2009; Allen et al. 2011), likely reflecting the mild trend with $L_{\rm Bol}$, due to the wider (by about one order of magnitude) quasar luminosity range sampled by these works. We conclude that the increasing trend of the BAL fraction at $z \gtrsim 6$ is a genuine cosmic evolution and does not depend either on trends with nuclear properties or on the S/N of the spectra.

5. Kinematic Properties of Broad Absorption Line Outflows

Here we investigate the evolution of the BAL kinematics across cosmic time, as traced by $v_{\rm max}$, $v_{\rm min}$, and $w_{\rm max}$ (Section 3.2). The top panel of Figure 8 shows that the maximum velocity of BAL outflows significantly increases by a factor of about 2 between $z \sim 2$–3 and $z \sim 6$ (p-value $\lesssim 2 \times 10^{-4}$; see Table 3), from $v_{\rm max} \sim$ 15,000 to ∼30,000 km s^{-1}. A similar trend is observed also for the minimum BAL velocity, reaching a typical value of $v_{\rm min} \sim$ 15,000 at $z \sim 6$. An increased fraction of BAL quasars with $v_{\rm max} \gtrsim$ 30,000 km s^{-1} at $z \sim 4$–4.5 was recently suggested by Rodríguez Hidalgo et al. (2020). Because of the larger increase of $v_{\rm max}$ with respect to $v_{\rm min}$ as a function of redshift, the width of the BAL features also increases between $z \sim 2$–3 (9000 km s^{-1}) and $z \sim 6$ (15,000 km s^{-1}).

Figure 9 shows that, because of the combination of the above trends, the composite spectrum of BAL quasars is differently affected by absorption features in three intervals of increasing redshift. The lowest redshift bin ($2.1 < z < 3.2$) shows that the absorption typically affects the blue side of C IV and the deepest absorption is located at 1500 Å (i.e., blueshifted by ∼9000 km s^{-1}). At intermediate redshift ($3.6 < z < 5.0$), the C IV wing is still partially altered by the absorption, which affects the whole spectral range between C IV and Si IV. The deepest absorption is blueshifted by ∼15,000 km s^{-1}. In the highest redshift interval ($5.8 < z < 6.6$), the absorption is even broader and extends blueward of Si IV, down to ∼1300 Å. The deepest absorption is blueshifted by ∼33,000 km s^{-1}. We note that, owing to the very broad distributions of $v_{\rm max}$and $v_{\rm min}$ in

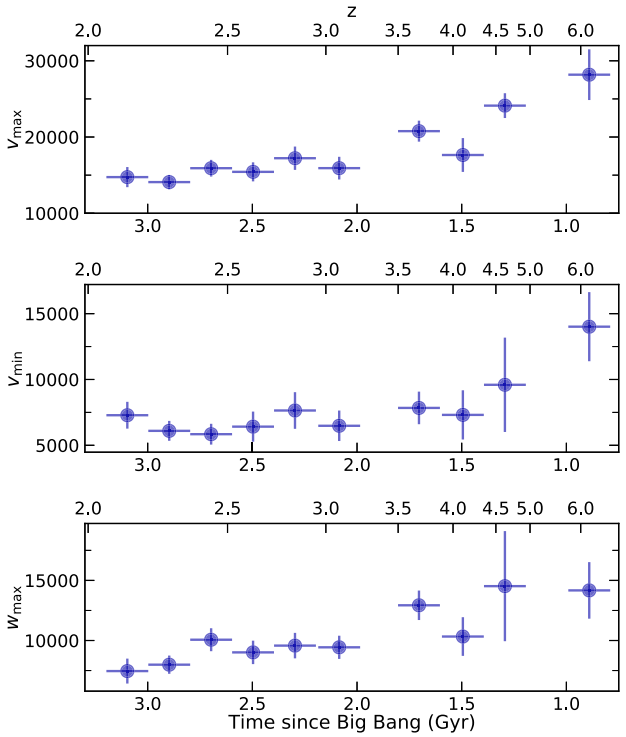

Figure 8. Maximum velocity (top), minimum velocity (middle), and maximum width (bottom) of the C IV BAL outflows, in units of kilometers per second, as a function of cosmic time. Top axes indicate the sampled redshift interval. Horizontal bars indicate the individual time bins of ∼200 Myr in which the average BAL velocity has been calculated. Vertical bars indicate the standard deviation error on the average value for each time bin.

combination with the small sample size in this high-redshift bin, we include in Figure 9 only BALs with the most prominent features (BI > 1000 km s^{-1}; Bischetti et al. 2022). These results, together with the higher BAL fraction observed in quasars at $5.8 < z < 6.6$, suggest an evolution of the BAL properties with cosmic time.

To test whether there is a dependence of the BAL kinematics on the nuclear quasar properties, we show in Figure 10 the relations between $v_{\rm max}$, $v_{\rm min}$, and $w_{\rm max}$ as a function of the BH accretion rate. We find no evident increase of either $v_{\rm max}$ and $v_{\rm min}$ with increasing $\lambda_{\rm Edd}$ over about two orders of magnitude, with an almost constant $v_{\rm max} \sim$ 15,000–17,000 km s^{-1} and $v_{\rm min} \sim$ 5000–7000 km s^{-1} (Table 3). There is a hint for a higher $w_{\rm max}$ (p-value ∼0.01–0.03) at high accretion rates, likely due to the lower $v_{\rm min}$ observed in the three bins with the highest $\lambda_{\rm Edd}$. Similarly, we observe no significant trend of the BAL kinematics with $L_{\rm Bol}$, likely due to the limited luminosity range spanned by our sample. Indeed, no or only mild trends of increasing $v_{\rm max}$ with $L_{\rm Bol}$ and $\lambda_{\rm Edd}$ were suggested by previous works studying BAL quasars in SDSS in a wider range of $L_{\rm Bol}$ (Ganguly et al. 2007; Gibson et al. 2009; Bruni et al. 2019). Previous studies at $z \sim 2$–4 reported tentative evidence of different properties in BAL quasars with low/high $v_{\rm min}$, in terms of the steepness of the X-ray to UV spectral energy distribution or emission-line properties, although no significant relation between $v_{\rm min}$ and quasar luminosity or accretion rate was found (Turnshek et al. 1988; Gibson et al. 2009). We agree with previous results finding no significant correlation between $v_{\rm min}$ and $\lambda_{\rm Edd}$ (Table 3). These findings confirm that the trend of increasing $v_{\rm min}$, $v_{\rm max}$, and $w_{\rm max}$ with redshift in our quasar

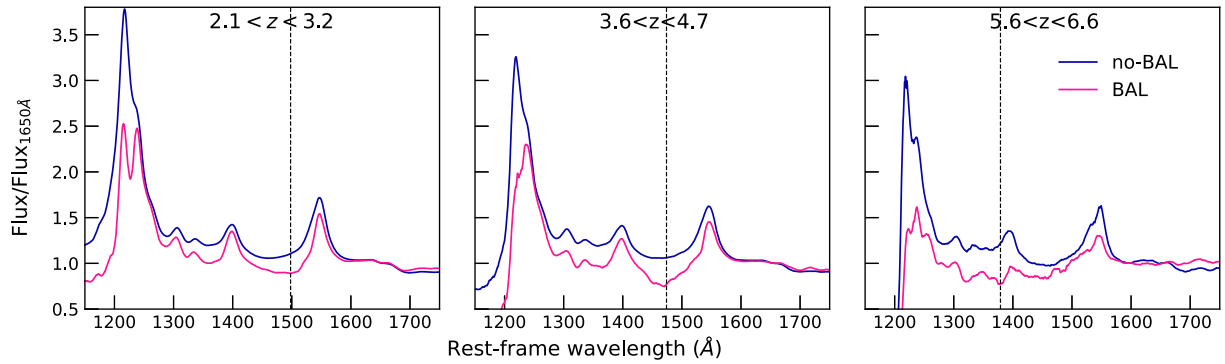

Figure 9. Composite template spectra of the BAL and non-BAL quasars in our sample, in three bins of increasing redshift (from left to right). For each panel, composite spectra have been normalized to the median continuum flux at 1600–1700 Å. The vertical line indicates the rest-frame wavelength corresponding to the maximum depth of the C IV absorption, showing a shift toward lower wavelengths with increasing redshift. In the right panel, we consider only quasars with prominent BAL features (BI $>$ 1000 km s^{-1}; Bischetti et al. 2022).

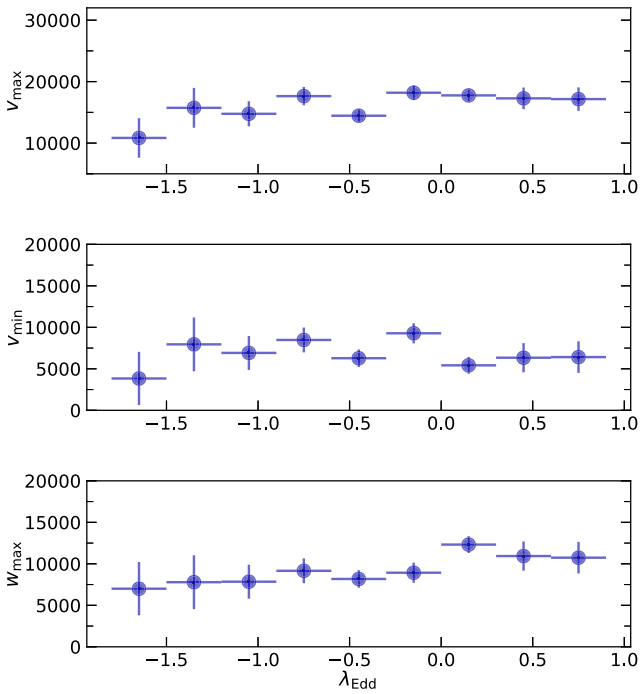

Figure 10. Maximum velocity (top), minimum velocity (middle), and maximum width (bottom) in units of kilometers per second, as a function of λ_{Edd} for the C IV BAL outflows in our quasar sample. Horizontal bars indicate the accretion rate bins in which the average BAL velocity has been calculated. Vertical bars indicate the standard deviation error on the average value for each bin.

sample cannot be explained by variations in the quasar nuclear properties, but rather points to an evolutionary effect.

6. Discussion

6.1. Cosmic Evolution of Broad Absorption Line Outflow Properties

Our results indicate an evolution with redshift of the properties of BAL outflows in luminous quasars at $2.1 < z < 6.8$. We find that the BAL fraction below $z \sim 4.5$ is almost constant and close to 20%–25% (Figure 7), while it significantly increases up to almost 50% at $z \sim 6$. The trend at $2.1 < z < 4.5$ is consistent with the results of previous studies focusing on rest-frame optical luminous quasar samples (Dai et al. 2008; Maddox et al. 2008), which reported a modest evolution of the BAL fraction with redshift. However, heavily reddened broad-line quasars are expected to represent a high fraction of the bright quasar population at $z > 2$ (Banerji et al. 2015; Glikman et al. 2018), and may be missed by SDSS, from which our $2.1 < z < 4.5$ sample is drawn. Several recent surveys (e.g., Schindler et al. 2019; Boutsia et al. 2021; Grazian et al. 2022) have indeed shown that the SDSS selection of bright quasars at high redshift could possibly suffer from incompleteness by up to 30%–40% at $z \sim 4$, and up to a factor of a few at $z \sim 5$ (Wolf et al. 2020; Onken et al. 2022), plausibly affecting also $z \sim 6$ quasars. Our $5.8 < z < 6.6$ quasar sample is limited to $J \leqslant 19.8$–20.0 magnitudes and probes similar depths in the J and WISE bands (see Table ED1 in Bischetti et al. 2022). Accordingly, we may miss red BAL quasars at $z \sim 6$, detected by WISE but too faint in the rest-frame UV to match our selection (e.g., Kato et al. 2020). Due to the above limitations and to the limited number of $z \gtrsim 5$ quasars in our sample, we cannot accurately probe the BAL fraction evolution in the highest-redshift bins. Nevertheless, we can safely assess that the increase in the BAL fraction between $z < 4.5$ and $z \sim 6$ is a robust evolutionary trend, and that selection effects (e.g., including dust-reddened quasars) would increase this difference even further.

By investigating the dependence of the BAL fraction on the quasar nuclear properties, we can safely exclude that the large difference between the BAL fraction at $z \lesssim 4.5$ and $z \sim 6$ is due to differences in quasar luminosity and accretion rate. Instead, the higher BAL fraction at $z \sim 6$ can be explained either with wider-angle outflows or as a result of longer blow-out phases of BH-driven outflows compared with $z \lesssim 4.5$ (Bischetti et al. 2022). A redshift evolution of the BAL geometry is indeed suggested by the increase with redshift of the velocity range spanned by the BAL troughs, as traced by w_{max} (Murray & Chiang 1998; Elvis 2000; Hall et al. 2002). Although the link of w_{max} to the velocity dispersion of the outflowing gas is not straightforward, as we mostly observe blends of outflowing components (e.g., Borguet et al. 2013), the increase of w_{max} may be interpreted as stronger turbulence in the higher-redshift BAL outflows. In a scenario of chaotic cold accretion (CCA), gas turbulence on scales similar to those of BALs (∼100 pc; Arav et al. 2018) is linked to the condensation and funnelling of the cold gas phase toward the BH, higher turbulence implying stronger inflows and, in turn, triggering more efficient phases of BH feedback (Gaspari et al. 2020).

We find that the BAL velocity (either v_{max} and v_{min}) typically increases with redshift, suggesting that BAL outflows in the high-z universe might be more easily accelerated to very high velocity than at later cosmic epochs. A viable explanation

might be the presence of dust mixed with the ionized gas in the BAL clouds, which would significantly increase the radiation boost efficiency (Ishibashi et al. 2017; Costa et al. 2018) and accelerate the BAL outflows to the observed extreme $v_{\rm max} \sim 20{,}000$–$50{,}000$ km s^{-1} (Bischetti et al. 2022). At later cosmic epochs, although BAL quasars are known to show relatively redder UV colors (Reichard et al. 2003; Trump et al. 2006; Gibson et al. 2009), no strong difference in the optical colors of BAL and non-BAL quasars is typically observed, at least in optically bright sources (e.g., Dai et al. 2008).

Alternative scenarios that could explain the higher BAL velocities at early epochs might be related to different properties of BH accretion at different redshift. CCA toward the BH is expected to be favored at higher redshift, because of a larger fraction of a clumpy cold gas phase in the quasar hosts, boosting BH-driven outflows to higher velocities (Gaspari & Sadowski 2017). Also, BALs could be launched with higher velocities if BHs are spinning more rapidly at high redshift (King et al. 2008; Zubovas & King 2021). High BAL velocities have been more commonly found in sources with softer spectral energy distributions, that is, lower X-ray to optical luminosity ratios, either from direct X-ray observations of low-z quasars (Laor & Brandt 2002) or using indirect tracers such as the EW of the He II λ1640 Å emission line in SDSS quasars (Richards et al. 2011; Baskin et al. 2015; Rodríguez Hidalgo et al. 2020). For the highest-redshift bins in which we observe the largest values of $v_{\rm max}$ and $v_{\rm min}$ (see Figure 8), there is very limited information on the X-ray properties. Only a few tens of quasars have been targeted with sensitive observations at $z > 5$, including only a few BAL quasars, some of which do exhibit the softest optical to X-ray slopes (Nanni et al. 2017; Vito et al. 2019; Wang et al. 2021a). The weakness of the He II emission line makes its detection very challenging at these redshifts (e.g., Shen et al. 2019). The characterization of the He II emission in the $5.8 < z < 6.6$ sample, enabled by the high S/N of the X-Shooter spectra from the XQR-30 survey, will be presented in a forthcoming paper.

6.2. Impact of Broad Absorption Line Outflows on Black Hole and Galaxy Evolution

The broad and often saturated BAL profiles associated with C IV prevent us from an accurate measurement of the outflowing gas mass and hence of the energy injected by the outflow into the galaxy medium (Dunn et al. 2012; Borguet et al. 2013). Nevertheless, assuming that BAL outflow masses at $z \sim 6$ are similar to those measured using unsaturated absorption lines in $z \sim 2$ quasars (Moe et al. 2009; Dunn et al. 2010), we can estimate that BAL quasars at $z \sim 6$ globally inject about 20 times more energy with respect to $z \sim 2$–4 quasars (Bischetti et al. 2022). Indeed, the outflow kinetic power linearly scales with the BAL fraction and with the third power of $v_{\rm max}$(Equations (5) and (6) in Bischetti et al. 2017). This result strongly points toward a phase of efficient BH feedback occurring at $z \sim 6$, as the energy injected by these BAL outflows will likely suppress gas accretion and slow down BH growth (e.g., Torrey et al. 2020). This likely represents the first observational evidence of what has been so far only predicted by cosmological simulations of the early assembly of bright quasars. BHs at the center of bright quasars are indeed expected to grow exponentially at very high redshift ($z \gg 6$), with accretion rates close to the Eddington limit or beyond (Inayoshi et al. 2016; Pezzulli et al. 2016), while around $z = 6$ BH growth is expected to significantly slow down because BH feedback has become strong enough to remove gas from the central galaxy regions and to prevent further accretion onto the BH (Costa et al. 2014; van der Vlugt & Costa 2019). BHs powering bright quasars at $z \sim 6$, with typical masses of $\sim 10^9\ M_\odot$ (Mazzucchelli et al. 2017; Shen et al. 2019; Farina et al. 2022), have been found to be typically overmassive by a factor of $\sim$10 with respect to the mass of their host galaxies, when compared to the BH mass versus galaxy dynamical mass relation observed in the low-redshift universe (Gaspari et al. 2019; Pensabene et al. 2020; Neeleman et al. 2021). State-of-the-art measurements of the BH mass (based on the Mg II line), and of the dynamical mass (based on spatially resolved C II λ158 μm observations) for the quasars in our $5.8 < z < 6.6$ sample confirm this result, indicating that BH growth must have dominated over the host-galaxy growth at $z >> 6$ and that a transition epoch during which BH growth decelerates must occur at $z \lesssim 6$, leading toward the symbiotic BH and galaxy growth (e.g., Lamastra et al. 2010; Zubovas & King 2021; Inayoshi et al. 2022). An early BH mass assembly in bright quasars occurring at $z > 6$ is also supported by the fact that the largest BH masses measured at $z \sim 6$ and at $z \sim 2$ only differ by a factor of a few (Trakhtenbrot 2021) and by the increase of the median BH accretion rate with redshift for a given quasar luminosity (Yang et al. 2021; Farina et al. 2022).

The above scenario points toward BH feedback as a likely driver of BH growth suppression, but other physical processes might be in place. The cosmic evolution of the BAL fraction is key to identify the dominant mechanism responsible for slowing down BH growth. A sharp decrease of the BAL fraction occurring between $z \sim 6$ and $z \sim 5$ would strongly point toward a phase of efficient BH feedback occurting on a short timescale (few tens of millions of years; Negri & Volonteri 2017) and quickly removing gas from the central regions of the galaxy (Zubovas & King 2013). Conversely, a smooth decrease of the BAL fraction from $z \sim 6$ to $z \sim 4$, would rather indicate that several processes may be at play in the transition, including a (less efficient) BH feedback and secular processes, such as a change in the merger rate or in the gas condensation rate, reducing the active phase duty cycle on a timescale of several hundreds of millions of years (Gaspari et al. 2019; O'Leary et al. 2021). To discriminate between these competing scenarios, a crucial step is to obtain a reliable measure of the evolution of the BAL fraction with redshift in representative samples, with a cosmic time sampling <100–200 Myr. Currently, the sample presented in this work and, particularly, the lack of sources at $5 < z < 5.8$ do not allow us to accurately probe the high-redshift evolution of the BAL fraction between $z \sim 4.5$ and $z \sim 6$. New high-quality spectroscopic observations of an absorption-unbiased sample of rest-frame optical bright quasars are necessary to fill this gap and test whether efficient BH feedback is the dominant mechanism leading to the symbiotic BH–galaxy growth phase.

On the other hand, it is unclear whether and on what timescales BAL outflows can affect the evolution of the host galaxies of $z \sim 6$ quasars. Observations of BAL quasars at intermediate redshift report mass outflow rates up to several hundreds of solar masses per year (e.g., Fiore et al. 2017; Bruni et al. 2019), consistent with theoretical expectations from models of BH-driven outflows for an efficient feedback mechanism (Faucher-Giguère & Quataert 2012; Zubovas & King 2012) and outflow sizes based on photoionization analysis that can reach kiloparsec scales (Arav et al. 2018; Byun et al. 2022), suggesting that BAL outflows may also affect the

physical properties of the galaxy medium and, in turn, the galaxy growth.

If the effect of BAL feedback extends to kiloparsec scales, host-galaxy properties such as the star formation rate (SFR) would be expected to be different in BAL and non-BAL quasars. If conflicting results have been reported at $z \sim 2$ (e.g., Zhang et al. 2014; Wethers et al. 2020) and at $z \sim 6$, large uncertainties affect SFR measurements (Wang et al. 2019; Tripodi et al. 2022; Di Mascia et al. 2023) and do not allow us to investigate differences within our $5.8 < z < 6.6$ sample. A correlation is also expected between the strength of BH feedback and the cooling rate of the hot and warm gas phases in the quasar host galaxies, due to heating and turbulence injection into the ISM (e.g., Gaspari 2015).

7. Conclusion

In this work, we analyze a sample of 1935 luminous (bolometric luminosity $L_{\rm bol} \gtrsim 10^{46.5}$ erg s^{-1}) quasars at $z = 2.1$–6.6, drawn from the SDSS (Shen et al. 2011) and from the X-Shooter legacy survey of Quasars at the Reionization Epoch (Bischetti et al. 2022), to investigate the evolution with cosmic time of the BAL fraction and of the kinematics of BH-driven outflows as traced by BAL features. Targeting rest-frame optical bright quasars allows us to to reduce biases due to quasar selection criteria (Section 2.1).

We apply a homogeneous BAL-identification method to the total sample, based on composite template spectra to estimate the intrinsic quasar continuum and line emission (Section 3). This approach allows us to well reproduce the spectral region between Lyα and C IV for a variety of BAL shapes, without any assumptions on the continuum shapes nor on the spectral regions in which absorption might occur. At the same time, it takes into account the asymmetry often observed in the C IV profile due to the presence of outflowing gas.

We find that the BAL fraction is about 20% and does not vary strongly across this redshift range, in agreement with previous works (Dai et al. 2008; Maddox et al. 2008), while it increases to almost 50% at $z \sim 6$ (Bischetti et al. 2022). We also investigate the dependence of the BAL fraction with quasar nuclear properties such as $L_{\rm Bol}$ and $\lambda_{\rm Edd}$, and we observe only weak correlations given the ranges of luminosity and accretion rate probed by our sample, in agreement with previous results for SDSS quasars (e.g., Gibson et al. 2009; Bruni et al. 2019). These trends cannot account for the increase in the BAL fraction observed in the $5.8 < z < 6.5$ sample (Section 4).

We also observe a redshift evolution of the BAL kinematics. Both $v_{\rm max}$ and $v_{\rm min}$ increases at $z \gtrsim 4$, the typical BAL velocities at $z \sim 6$ being a factor of 2–3 higher than what is observed at $z < 4$ (Section 5). The width of the BAL features also likely increases at $z \gtrsim 4$. These trends suggest a possible evolution of the BAL geometry and are consistent with BALs being more easily accelerated at early cosmic epochs (Section 6.1). By investigating the dependence of the BAL kinematics with $L_{\rm Bol}$ and $\lambda_{\rm Edd}$, we were able to exclude that the redshift evolution is due to different luminosity and/or accretion properties within the sample.

BAL outflows being more common and faster at $z \sim 6$ imply that strong BH feedback is likely occurring around this epoch, owing to the injection of large amounts of energy into the BH surroundings and in the galaxy medium, in agreement with expectations from galaxy-evolution models (van der Vlugt & Costa 2019; Inayoshi et al. 2022). However, the limited number of high-redshift quasars in our sample does not allow us to accurately probe the $z \gtrsim 4.5$ evolution of the BAL fraction on a timescale of 100–200 Myr. This hampers us from discriminating between a sudden or a smooth change of the BAL fraction with increasing redshift and, in turn, from assessing whether BH feedback is driving this evolution. Building a larger, absorption-unbiased sample of rest-frame optical bright quasars with high-quality optical and near-IR spectroscopy will be fundamental to observationally quantify the impact of BH feedback on early BH growth. By complementing this sample with high-frequency Atacama Large Millimeter/submillimeter Array and JWST observations, we will be able to measure the host-galaxy growth and to assess whether quasar feedback at $z \sim 6$ drives the onset of the symbiotic BH and galaxy evolution observed in the lower-redshift universe.

Acknowledgments

This work is based on observations collected at the European Organisation for Astronomical Research in the Southern Hemisphere under ESO large program 1103.A-0817(A). Funding for SDSS and SDSS-II has been provided by the Alfred P. Sloan Foundation, the Participating Institutions, the National Science Foundation, the US Department of Energy, the National Aeronautics and Space Administration, the Japanese Monbukagakusho, the Max Planck Society and the Higher Education Funding Council for England. The SDSS website is http://www.sdss.org/. The SDSS is managed by the Astrophysical Research Consortium for the Participating Institutions. The Participating Institutions are the American Museum of Natural History, the Astrophysical Institute Potsdam, the University of Basel, the University of Cambridge, Case Western Reserve University, the University of Chicago, Drexel University, Fermilab, the Institute for Advanced Study, the Japan Participation Group, Johns Hopkins University, the Joint Institute for Nuclear Astrophysics, the Kavli Institute for Particle Astrophysics and Cosmology, the Korean Scientist Group, the Chinese Academy of Sciences (LAMOST), Los Alamos National Laboratory, the Max-Planck-Institute for Astronomy, the Max-Planck-Institute for Astrophysics, New Mexico State University, Ohio State University, the University of Pittsburgh, the University of Portsmouth, Princeton University, the United States Naval Observatory, and the University of Washington. M.B., acknowledges support from the INAF MINI-GRANT SNR1 "Mini-feedback" - 1.05.12.04.01. M.B., C.F., and F.F. acknowledge support from the PRIN MIUR project "Black Hole winds and the Baryon Life Cycle of Galaxies: the stone-guest at the galaxy evolution supper," contract number 2017PH3WAT. M.G. acknowledges partial support by HST grant No. GO-15890.020/023-A and the BlackHoleWeather program. K.Z. acknowledges support by the Research Council Lithuania grant No. S-MIP-20-43. E.P.F. is supported by the international Gemini Observatory, a program of NSF's NOIRLab, which is managed by the Association of Universities for Research in Astronomy (AURA) under a cooperative agreement with the National Science Foundation, on behalf of the Gemini partnership of Argentina, Brazil, Canada, Chile, the Republic of Korea, and the United States of America.

Facilities: VLT(UT2 X-Shooter), Sloan.

Software: python 3.8 (Van Rossum & Drake 2009), numpy (Harris et al. 2020), astropy (Astropy Collaboration et al. 2013; Collaboration et al. 2018), pandas (McKinney 2010; Reback & McKinney 2020), matplotlib (Hunter 2007).

Appendix

In this appendix we present the X-shooter spectra of all quasars in our $5.8 < z < 6.6$ sample from the XQR-30 survey (Figure 11). For each quasar, we also show the best-fit composite template, created as described in Section 3.1, which we used to calculate the residual spectra and identify BAL features (Section 3.4). Figure 12 displays the residual spectra of the $5.8 < z < 6.6$ BAL quasars in which we identified absorption features associated with Si IV and N V ions (Table 2), in addition to the C IV BAL features presented in Bischetti et al. (2022).

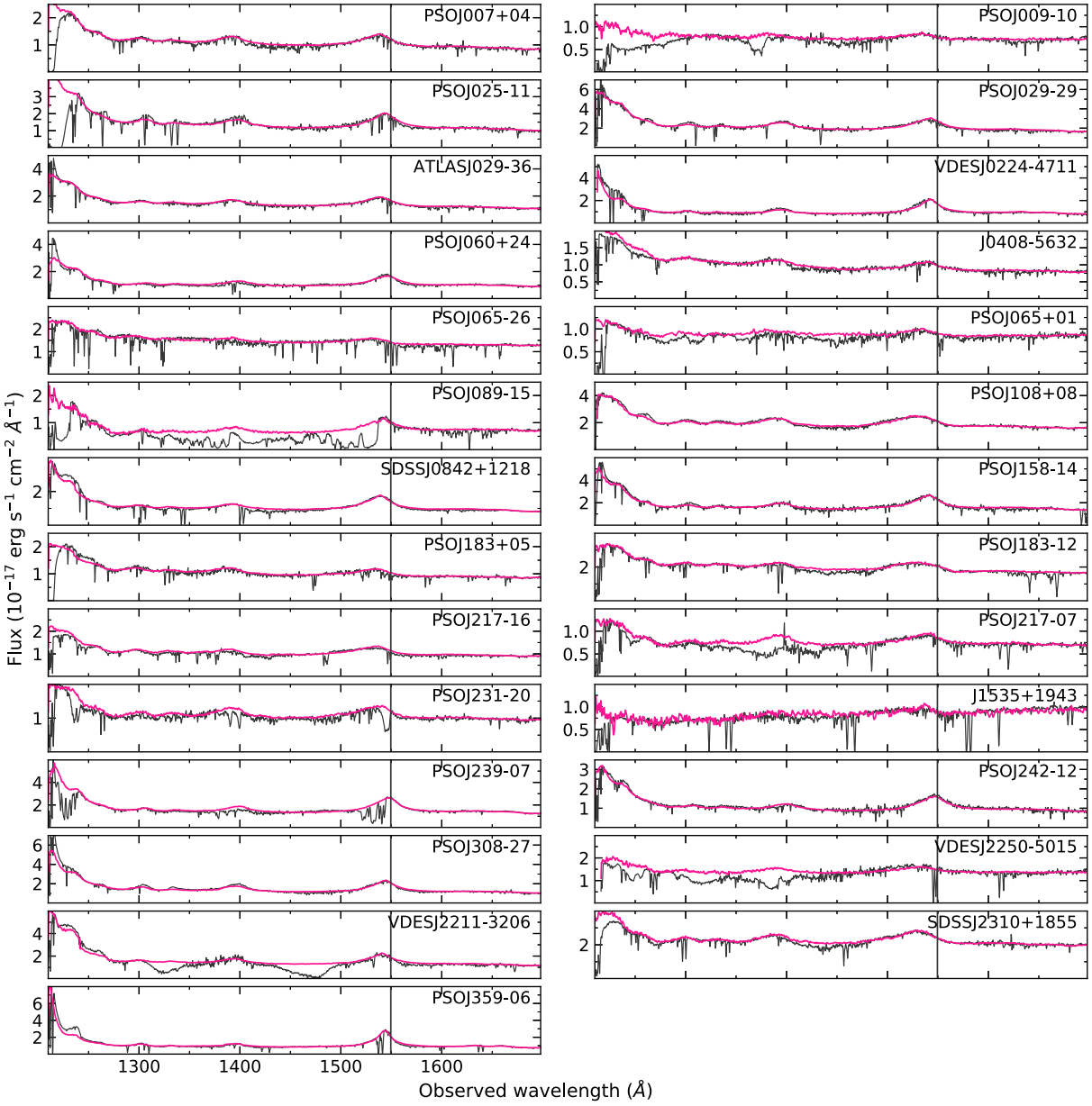

Figure 11. X-Shooter spectra of the $5.8 < z < 6.6$ quasars in our sample (black curves), binned to 150 km s^{-1}. Composite templates, used to estimate the intrinsic quasar emission, are shown by the magenta curve. The vertical line indicates the rest-frame wavelength of C IV.

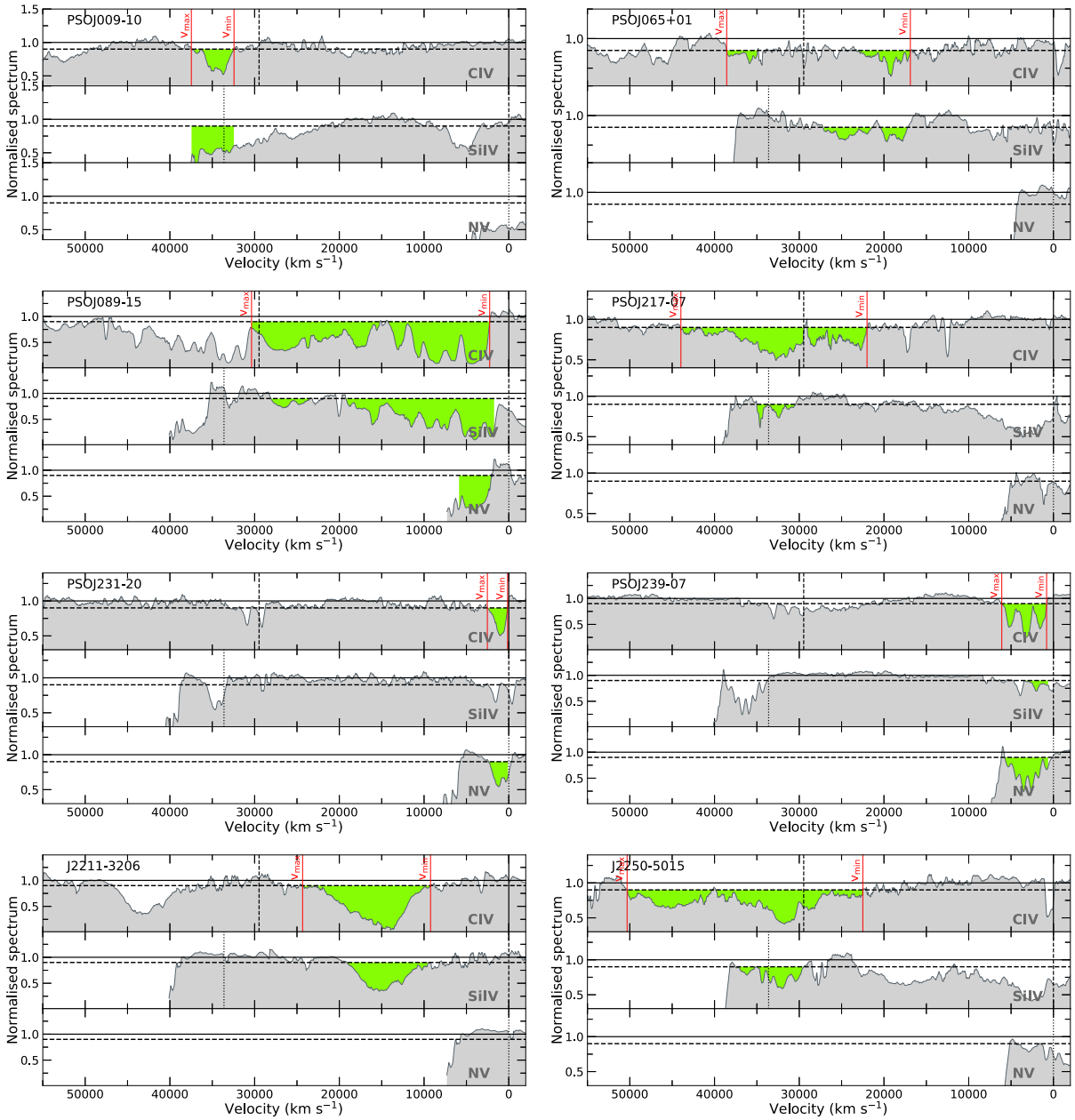

Figure 12. Normalized spectra for the BAL quasars identified in the $5.8 < z < 6.6$ sample, smoothed to 500 km s^{-1}. The velocity axis in each panel is relative to the rest-frame wavelength of the ionic species indicated by the label. Vertical solid, dashed, and dotted lines indicate the velocity associated with C IV, Si IV, and N V emission lines, respectively. The solid (dashed) horizontal line represents a flux level of 1.0 (0.9). BAL troughs, corresponding to a flux level <0.9 (Equation (1)), are highlighted as green shaded areas.

ORCID iDs

Manuela Bischetti https://orcid.org/0000-0002-4314-021X
Fabrizio Fiore https://orcid.org/0000-0002-4031-4157
Chiara Feruglio https://orcid.org/0000-0002-4227-6035
Valentina D'Odorico https://orcid.org/0000-0003-3693-3091
Nahum Arav https://orcid.org/0000-0003-2991-4618
Tiago Costa https://orcid.org/0000-0002-6748-2900
Kastytis Zubovas https://orcid.org/0000-0002-9656-6281
George Becker https://orcid.org/0000-0003-2344-263X
Sarah E. I. Bosman https://orcid.org/0000-0001-8582-7012
Guido Cupani https://orcid.org/0000-0002-6830-9093
Rebecca Davies https://orcid.org/0000-0002-3324-4824
Anna-Christina Eilers https://orcid.org/0000-0003-2895-6218
Emanuele Paolo Farina https://orcid.org/0000-0002-6822-2254
Andrea Ferrara https://orcid.org/0000-0002-9400-7312
Massimo Gaspari https://orcid.org/0000-0003-2754-9258
Chiara Mazzucchelli https://orcid.org/0000-0002-5941-5214
Masafusa Onoue https://orcid.org/0000-0003-2984-6803
Enrico Piconcelli https://orcid.org/0000-0001-9095-2782
Maria Vittoria Zanchettin https://orcid.org/0000-0001-7883-496X
Yongda Zhu https://orcid.org/0000-0003-3307-7525

References

Allen, J. T., Hewett, P. C., Maddox, N., Richards, G. T., & Belokurov, V. 2011, ApJ, 410, 860
Arav, N., Liu, G., Xu, X., et al. 2018, ApJ, 857, 60
Astropy Collaboration, Price-Whelan, A. M., Sipőcz, B. M., et al. 2018, AJ, 156, 123
Astropy Collaboration, Robitaille, T. P., Tollerud, E. J., et al. 2013, A&A, 558, A33
Bañados, E., Venemans, B. P., Decarli, R., et al. 2016, ApJS, 227, 11
Banerji, M., Alaghband-Zadeh, S., Hewett, P. C., & McMahon, R. G. 2015, MNRAS, 447, 3368
Baskin, A., Laor, A., & Hamann, F. 2015, MNRAS, 449, 1593
Becker, G. D., Pettini, M., Rafelski, M., et al. 2019, ApJ, 883, 163
Becker, R. H., White, R. L., Gregg, M. D., et al. 2000, ApJ, 538, 72
Bischetti, M., Feruglio, C., D'Odorico, V., et al. 2022, Natur, 605, 244
Bischetti, M., Piconcelli, E., Vietri, G., et al. 2017, A&A, 598, A122
Borguet, B. C. J., Arav, N., Edmonds, D., Chamberlain, C., & Benn, C. 2013, ApJ, 762, 49
Bosman, S. E. I., Davies, F. B., Becker, G. D., et al. 2022, MNRAS, 514, 55
Boutsia, K., Grazian, A., Fontanot, F., et al. 2021, ApJ, 912, 111
Bruni, G., Piconcelli, E., Misawa, T., et al. 2019, A&A, 630, A111
Byun, D., Arav, N., & Hall, P. B. 2022, ApJ, 927, 176
Chehade, B., Carnall, A. C., Shanks, T., et al. 2018, MNRAS, 478, 1649
Chen, Z., He, Z., Ho, L. C., et al. 2022, NatAs, 6, 339
Coatman, L., Hewett, P. C., Banerji, M., et al. 2017, MNRAS, 465, 2120
Costa, T., Rosdahl, J., Sijacki, D., & Haehnelt, M. G. 2018, MNRAS, 473, 4197
Costa, T., Sijacki, D., Trenti, M., & Haehnelt, M. G. 2014, MNRAS, 439, 2146
Dai, X., Shankar, F., & Sivakoff, G. R. 2008, ApJ, 672, 108
Decarli, R., Walter, F., Venemans, B. P., et al. 2018, ApJ, 854, 97
Di Mascia, F., Carniani, S., Gallerani, S., et al. 2023, MNRAS, 518, 3667
Dunn, J. P., Arav, N., Aoki, K., et al. 2012, ApJ, 750, 143
Dunn, J. P., Crenshaw, D. M., Kraemer, S. B., & Trippe, M. L. 2010, ApJ, 713, 900
Eilers, A.-C., Hennawi, J. F., Decarli, R., et al. 2020, ApJ, 900, 37
Elvis, M. 2000, ApJ, 545, 63
Farina, E. P., Schindler, J.-T., Walter, F., et al. 2022, ApJ, 941, 106
Faucher-Giguère, C.-A., & Quataert, E. 2012, MNRAS, 425, 605
Filiz, A. N., Brandt, W. N., Hall, P. B., et al. 2014, ApJ, 791, 88
Fiore, F., Feruglio, C., Shankar, F., et al. 2017, A&A, 601, A143
Gallerani, S., Maiolino, R., Juarez, Y., et al. 2010, A&A, 523, A85
Ganguly, R., & Brotherton, M. S. 2008, ApJ, 672, 102
Ganguly, R., Brotherton, M. S., Cales, S., et al. 2007, ApJ, 665, 990
Gaspari, M. 2015, MNRAS Lett., 451, L60
Gaspari, M., Eckert, D., Ettori, S., et al. 2019, ApJ, 884, 169
Gaspari, M., & Sadowski, A. 2017, ApJ, 837, 149
Gaspari, M., Tombesi, F., & Cappi, M. 2020, NatAs, 4, 10
Gehrels, N. 1986, ApJ, 303, 336
Gibson, R. R., Jiang, L., Brandt, W. N., et al. 2009, ApJ, 692, 758
Giustini, M., Cappi, M., & Vignali, C. 2008, A&A, 491, 425
Glikman, E., Lacy, M., LaMassa, S., et al. 2018, ApJ, 861, 37
Glikman, E., Lacy, M., Urrutia, T., Djorgovski, G., & Mahabal, A. 2012, AAS Meeting Abstracts, 219, 209.03
Grazian, A., Giallongo, E., Boutsia, K., et al. 2022, ApJ, 924, 62
Guo, Z., & Martini, P. 2019, ApJ, 879, 72
Hall, P. B., Anderson, S. F., Strauss, M. A., et al. 2002, ApJS, 141, 267
Hamann, F., Chartas, G., Reeves, J., & Nardini, E. 2018, MNRAS, 476, 943
Harris, C. R., Millman, K. J., van der Walt, S. J., et al. 2020, Natur, 585, 357
Hemler, Z. S., Grier, C. J., Brandt, W. N., et al. 2019, ApJ, 872, 21
Hewett, P. C., & Foltz, C. B. 2003, AJ, 125, 1784
Hunter, J. D. 2007, CSE, 9, 90
Inayoshi, K., Haiman, Z., & Ostriker, J. P. 2016, MNRAS, 459, 3738
Inayoshi, K., Nakatani, R., Toyouchi, D., et al. 2022, ApJ, 927, 237
Ishibashi, W., Banerji, M., & Fabian, A. C. 2017, MNRAS, 469, 1496
Kakkad, D., Mainieri, V., Vietri, G., et al. 2020, A&A, 642, A147
Kato, N., Matsuoka, Y., Onoue, M., et al. 2020, PASJ, 72, 84
King, A. R., Pringle, J. E., & Hofmann, J. A. 2008, MNRAS, 385, 1621
Knigge, C., Scaringi, S., Goad, M. R., & Cottis, C. E. 2008, MNRAS, 386, 1426
Kurk, J. D., Walter, F., Fan, X., et al. 2007, ApJ, 669, 32
Lai, S., Bian, F., Onken, C. A., et al. 2022, MNRAS, 513, 1801
Lamastra, A., Menci, N., Maiolino, R., Fiore, F., & Merloni, A. 2010, MNRAS, 405, 29
Laor, A., & Brandt, W. N. 2002, ApJ, 569, 641
Maddox, N., Hewett, P. C., Warren, S. J., & Croom, S. M. 2008, MNRAS, 386, 1605
Maiolino, R., Oliva, E., Ghinassi, F., et al. 2004, A&A, 420, 889
Marconi, A., Risaliti, G., Gilli, R., et al. 2004, MNRAS, 351, 169
Mazzucchelli, C., Bañados, E., Venemans, B. P., et al. 2017, ApJ, 849, 91
McKinney, W. 2010, in Proc. the 9th Python in Sci. Conf. (Austin, TX: SciPy), 56
Menci, N., Fiore, F., Feruglio, C., et al. 2019, ApJ, 877, 74
Meyer, R. A., Bosman, S. E. I., & Ellis, R. S. 2019, MNRAS, 487, 3305
Moe, M., Arav, N., Bautista, M. A., & Korista, K. T. 2009, ApJ, 706, 525
Murray, N., & Chiang, J. 1998, ApJ, 494, 125
Nanni, R., Vignali, C., Gilli, R., Moretti, A., & Brandt, W. N. 2017, A&A, 603, A128
Neeleman, M., Novak, M., Venemans, B. P., et al. 2021, ApJ, 911, 141
Negri, A., & Volonteri, M. 2017, MNRAS, 467, 3475
O'Leary, J. A., Moster, B. P., Naab, T., & Somerville, R. S. 2021, MNRAS, 501, 3215
Onken, C. A., Wolf, C., Bian, F., et al. 2022, MNRAS, 511, 572
Pâris, I., Petitjean, P., Aubourg, É., et al. 2018, A&A, 613, A51
Pensabene, A., Carniani, S., Perna, M., et al. 2020, A&A, 637, A84
Pezzulli, E., Valiante, R., & Schneider, R. 2016, MNRAS, 458, 3047
Planck Collaboration, Ade, P. A. R., Aghanim, N., et al. 2016, A&A, 594, A13
Proga, D., & Kallman, T. R. 2004, ApJ, 616, 688
Proga, D., Stone, J. M., & Kallman, T. R. 2000, ApJ, 543, 686
Reback, J., McKinney, W., jbrockmendel, et al. 2020, pandas-dev/pandas: Pandas v1.1.3, Zenodo, doi:10.5281/zenodo.4067057
Reed, S. L., McMahon, R. G., Martini, P., et al. 2017, MNRAS, 468, 4702
Reichard, T. A., Richards, G. T., Hall, P. B., et al. 2003, AJ, 126, 2594
Richards, G. T., Fan, X., Newberg, H. J., et al. 2002, AJ, 123, 2945
Richards, G. T., Kruczek, N. E., Gallagher, S. C., et al. 2011, AJ, 141, 167
Richards, G. T., Lacy, M., Storrie-Lombardi, L. J., et al. 2006, ApJS, 166, 470
Rodríguez Hidalgo, P., Khatri, A. M., Hall, P. B., et al. 2020, ApJ, 896, 151
Ross, N. P., & Cross, N. J. G. 2020, MNRAS, 494, 789
Runnoe, J. C., Brotherton, M. S., & Shang, Z. 2012, MNRAS, 426, 2677
Sadowski, A., & Gaspari, M. 2017, MNRAS, 468, 1398
Schindler, J.-T., Fan, X., McGreer, I. D., et al. 2019, ApJ, 871, 258
Schindler, J.-T., Farina, E. P., Bañados, E., et al. 2020, ApJ, 905, 51
Schneider, D. P., Hall, P. B., Richards, G. T., et al. 2007, AJ, 134, 102
Shen, Y., Richards, G. T., Strauss, M. A., et al. 2011, ApJS, 194, 45
Shen, Y., Wu, J., Jiang, L., et al. 2019, ApJ, 873, 35
Skrutskie, M. F., Cutri, R. M., Stiening, R., et al. 2006, AJ, 131, 1163
Smette, A., Sana, H., Noll, S., et al. 2015, A&A, 576, A77
Torrey, P., Hopkins, P. F., Faucher-Giguère, C.-A., et al. 2020, MNRAS, 497, 5292
Trakhtenbrot, B. 2021, in IAU Symp. 365, Nuclear Activity in Galaxies Across Cosmic Time, ed. M. Pović et al. (Cambridge: Cambridge Univ. Press), 261
Tripodi, R., Feruglio, C., Fiore, F., et al. 2022, A&A, 665, A107
Trump, J. R., Hall, P. B., Reichard, T. A., et al. 2006, ApJS, 165, 1
Turnshek, D. A., Foltz, C. B., Grillmair, C. J., & Weymann, R. J. 1988, ApJ, 325, 651
Urrutia, T., Lacy, M., & Becker, R. H. 2008, ApJ, 674, 80
van der Vlugt, D., & Costa, T. 2019, MNRAS, 490, 4918
Van Rossum, G., & Drake, F. L. 2009, Python 3 Reference Manual (Scotts Valley: CA: CreateSpace)
Vestergaard, M., & Osmer, P. S. 2009, ApJ, 699, 800
Vietri, G., Misawa, T., Piconcelli, E., et al. 2022, A&A, 668, A87
Vietri, G., Piconcelli, E., Bischetti, M., et al. 2018, A&A, 617, A81
Vito, F., Brandt, W. N., Bauer, F. E., et al. 2019, A&A, 630, A118
Volonteri, M., & Rees, M. J. 2006, ApJ, 650, 669
Wang, F., Fan, X., Yang, J., et al. 2021a, ApJ, 908, 53
Wang, F., Yang, J., Fan, X., et al. 2018, ApJL, 869, L9
Wang, F., Yang, J., Fan, X., et al. 2019, ApJ, 884, 30
Wang, F., Yang, J., Fan, X., et al. 2021b, ApJL, 907, L1
Warren, S. J., Hambly, N. C., Dye, S., et al. 2007, MNRAS, 375, 213
Wethers, C. F., Kotilainen, J., Schramm, M., & Schulze, A. 2020, MNRAS, 498, 1469
Weymann, R. J., Morris, S. L., Foltz, C. B., & Hewett, P. C. 1991, ApJ, 373, 23
Wolf, C., Hon, W. J., Bian, F., et al. 2020, MNRAS, 491, 1970
Wright, E. L., Eisenhardt, P. R. M., Mainzer, A. K., et al. 2010, AJ, 140, 1868
Xu, X., Zakamska, N. L., Arav, N., Miller, T., & Benn, C. 2020, MNRAS, 495, 305
Yang, J., Wang, F., Fan, X., et al. 2021, ApJ, 923, 262
Zakamska, N. L., Hamann, F., Pâris, I., et al. 2016, MNRAS, 459, 3144
Zeilig-Hess, M., Levinson, A., Xu, X., & Arav, N. 2020, MNRAS, 491, 4325
Zhang, S., Wang, H., Wang, T., et al. 2014, ApJ, 786, 42
Zhu, Y., Becker, G. D., Bosman, S. E. I., et al. 2022, ApJ, 932, 76
Zhu, Y. L., Lund, K. A., Barnes, J., et al. 2021, ApJ, 906, 94
Zubovas, K., & King, A. 2012, ApJL, 745, L34
Zubovas, K., & King, A. 2013, ApJ, 769, 51
Zubovas, K., & King, A. 2021, MNRAS, 501, 4289